Published for SISSA by Springer

Received: *January 23, 2024*
Accepted: *March 25, 2024*
Published: *April 19, 2024*

Prompt and nonprompt $\psi(2S)$ production in pPb collisions at $\sqrt{s_{\rm NN}} = 8.16$ TeV

The LHCb collaboration

E-mail: patrick.robbe@ijclab.in2p3.fr

Abstract: The production of $\psi(2S)$ mesons in proton-lead collisions at a centre-of-mass energy per nucleon pair of $\sqrt{s_{\rm NN}} = 8.16$ TeV is studied with the LHCb detector using data corresponding to an integrated luminosity of $34\,{\rm nb}^{-1}$. The prompt and nonprompt $\psi(2S)$ production cross-sections and the ratio of the $\psi(2S)$ to J/ψ cross-section are measured as a function of the meson transverse momentum and rapidity in the nucleon-nucleon centre-of-mass frame, together with forward-to-backward ratios and nuclear modification factors. The production of prompt $\psi(2S)$ is observed to be more suppressed compared to pp collisions than the prompt J/ψ production, while the nonprompt productions have similar suppression factors.

Keywords: QCD, Heavy Quark Production, Particle and Resonance Production, Hadron-Hadron Scattering

ArXiv ePrint: 2401.11342

https://doi.org/10.1007/JHEP04(2024)111

Contents

1 Introduction

The study of quark-gluon plasma (QGP) requires a broad range of observables. Amongst many potential probes likely to be affected by the presence of a colour-deconfined medium, quarkonium states such as J/ψ and $\psi(2S)$ were first proposed by Matsui and Satz in 1986 [1]. The charm and anticharm quark pairs produced in hard scattering processes are expected to be dissociated by colour screening in the presence of QGP, which would lead to a suppression of J/ψ and $\psi(2S)$ production in heavy-ion collisions relative to production in proton-proton collisions. The theoretical understanding of the quarkonium bound-state dynamics has

JHEP04(2024)111

improved significantly over the past 30 years [2], with the development of lattice quantum chromodynamics (QCD) and effective field theory approaches, and experimental measurements at the SPS, RHIC and LHC accelerators reveal patterns indicative of deconfinement [3]. More specifically, a low transverse-momentum contribution to J/ψ production was observed at the LHC [4–8], which has been interpreted as a signature of charmonium production originating from recombination of unbound charm quarks generated either during the lifetime of the deconfined medium [9] or at the phase boundary [10].

In this context, the measurement of $\psi(2S)$ meson production in heavy-nucleus collisions, and its comparison with J/ψ production, plays a crucial role in the interpretation of charmonium measurements. The $\psi(2S)$ state has a larger spatial extension and a smaller binding energy than the J/ψ state [11]. In addition, its production does not contain feed-down contributions from decays of χ_c states, in contrast to the J/ψ case. Uncertainties in the predicted overall charm cross-section cancel out in the ratio of $\psi(2S)$ to J/ψ production in nucleus-nucleus collisions. The charmonium production ratio constitutes an observable that can constrain or discriminate between theoretical models [12]. First measurements of the $\psi(2S)$ to J/ψ production ratio in nucleus-nucleus collisions at the LHC have been performed by the CMS [13–15], ALICE [7, 16] and ATLAS [17] collaborations, at center of mass per nucleon pair energies of $\sqrt{s_{\rm NN}} = 2.76\,\text{TeV}$ and $5.20\,\text{TeV}$.

Effects that are not related to deconfinement, known as cold nuclear matter (CNM) effects, play an important role in the interpretation of the available data from ultra-relativistic nucleus-nucleus collisions. An accurate quantification of the CNM effects is necessary to distinguish them from deconfinement-related phenomena. The size of the CNM effects can be measured in proton-nucleus or deuteron-nucleus collisions, which have been studied at various collision energies [3]. At the LHC collision energies, the main modifications of charmonium production compared to pp collisions are related to the modification of the gluon flux. This is treated using collinear factorisation with nuclear parton distribution functions (nPDFs) [18–22] or using the colour glass condensate (CGC) approach to describe the saturation regime of QCD [23, 24]. Furthermore, small-angle gluon radiation arising from the interference between initial and final-state radiation, called coherent energy loss, was proposed as one of the dominant causes of nuclear modification in quarkonium production in proton-nucleus collisions [25]. Calculations based on these approaches [25–30] are able to describe J/ψ production measurements at the LHC [31–37] reasonably well within their respective uncertainties. In these computations, the slightly different kinematics induced by the mass difference between the J/ψ and the $\psi(2S)$ states and the feed-down originating from χ_c decays contributing to the J/ψ production are considered negligible compared to the uncertainties in the models themselves. The modification of quarkonium production in these models affects the initial state only but not the J/ψ or $\psi(2S)$ final states, that is to say identical modification of the production of these two mesons is predicted. In contrast to these phenomenological expectations, indications of a relative suppression of $\psi(2S)$ meson production with respect to the production of the J/ψ meson were observed by the PHENIX collaboration at RHIC [38, 39] in proton-nucleus or deuteron-nucleus collisions at $\sqrt{s_{\rm NN}}$ =200 GeV and by the ALICE [40–43], CMS [44] and LHCb [45] collaborations at the LHC in proton-nucleus collisions at $\sqrt{s_{\rm NN}}$ =5.02 TeV and 8.16 TeV.

JHEP04(2024)111

This study aims to improve the understanding of the relative production of $\psi(2S)$ and J/ψ in proton-nucleus compared to pp collisions. The similar previous measurement by the LHCb collaboration [45] did not have sufficient precision to draw conclusions on the relative suppression between the two states. The analysis separates prompt and nonprompt production, where the former consists of mesons produced directly in the collisions or in decays of higher-mass promptly-produced charmonium states, and the latter consists of mesons produced in decays of b-hadrons. Comparisons with models including factorisation breaking via hadronic or partonic interactions influencing the fate of the $c\bar{c}$ pair after its creation [46, 47] are provided.

2 Detector, data sample and observables

The LHCb detector [48, 49] is a single-arm forward spectrometer covering the pseudorapidity range $2 < \eta < 5$, designed for the study of particles containing b or c quarks. The detector includes a high-precision tracking system consisting of a silicon-strip vertex detector surrounding the interaction region [50], a large-area silicon-strip detector located upstream of a dipole magnet with a bending power of about 4 Tm, and three stations of silicon-strip detectors and straw drift tubes [51] placed downstream of the magnet. The tracking system provides a measurement of the momentum of charged particles with a relative uncertainty that varies from 0.5% at low momentum to 1.0% at 200 GeV/c. The minimum distance of a track to a primary vertex (PV), the impact parameter, is measured with a resolution of $(15 + 29/p_{\mathrm{T}})$ µm, where p_{T} is the transverse momentum in the LHCb frame, in GeV/c. Different types of charged hadrons are distinguished using information from two ring-imaging Cherenkov detectors [52]. Photons, electrons and hadrons are identified by a calorimeter system consisting of scintillating-pad and preshower detectors, an electromagnetic calorimeter and a hadronic calorimeter. Muons are identified by a system composed of alternating layers of iron and multiwire proportional chambers [53].

This analysis is based on data acquired during the 2016 LHC heavy-ion run with collisions of protons and ^{208}Pb ions at a centre-of-mass energy per nucleon pair of $\sqrt{s_{\mathrm{NN}}} = 8.16$ TeV. During the run, the direction of the ion and proton beams were exchanged in the accelerator and data recorded with these two different configurations. Since the energy per nucleon in the proton beam is larger than in the lead beam, the nucleon-nucleon centre-of-mass system has a rapidity in the laboratory frame of 0.465 (-0.465), when the proton (lead) beam travels from the vertex detector towards the muon chambers. Consequently, the LHCb detector covers two different acceptance regions,

- $1.5 < y^* < 4.0$ when the proton beam travels from the vertex detector towards the muon chambers, denoted pPb, and
- $-5.0 < y^* < -2.5$ when the proton beam travels from the muon chambers towards the vertex detector, denoted Pbp,

where y^* is the rapidity in the centre-of-mass frame of the colliding nucleons with respect to the proton beam direction. The data samples correspond to an integrated luminosity of $13.6 \pm 0.3\,\mathrm{nb}^{-1}$ of pPb collisions and $20.8 \pm 0.5\,\mathrm{nb}^{-1}$ of Pbp collisions [54]. The instantaneous

JHEP04(2024)111

luminosity while these samples were recorded ranged between 0.5 and $1.0 \times 10^{29}\,\mathrm{cm}^{-2}\mathrm{s}^{-1}$, where the average number of collisions per bunch crossing is less than 0.1.

3 Definition of the observables

The differential prompt and nonprompt production cross-sections for $\psi(2S)$ mesons are measured in the range $0 < p_{\mathrm{T}} < 14\,\mathrm{GeV}/c$ and $1.5 < y^* < 4.0$ for pPb collisions and $-5.0 < y^* < -2.5$ for Pbp collisions, in bins of p_{T} and y^*. The $\psi(2S)$ to J/ψ cross-section ratio

$$\frac{\mathrm{d}^2\sigma_{\psi(2S)}/\mathrm{d}p_{\mathrm{T}}\mathrm{d}y^*}{\mathrm{d}^2\sigma_{J/\psi}/\mathrm{d}p_{\mathrm{T}}\mathrm{d}y^*} = \frac{N(\psi(2S))}{N(J/\psi)} \times \frac{\epsilon^{\mathrm{tot}}(J/\psi)}{\epsilon^{\mathrm{tot}}(\psi(2S))} \times \frac{\mathcal{B}\left(J/\psi \to \mu^+\mu^-\right)}{\mathcal{B}\left(\psi(2S) \to e^+e^-\right)} \tag{3.1}$$

is obtained from the ratio of measured $\psi(2S)$ to J/ψ yields in the same dataset, $N(\psi(2S))$ and $N(J/\psi)$, reconstructed in the $\mu^+\mu^-$ final state, corrected for acceptance and detection efficiencies, $\epsilon^{\mathrm{tot}}(\psi(2S))$ and $\epsilon^{\mathrm{tot}}(J/\psi)$, and for the branching fractions into $\mu^+\mu^-$, $\mathcal{B}\left(\psi(2S) \to e^+e^-\right) = (7.93 \pm 0.17) \times 10^{-3}$ and $\mathcal{B}\left(J/\psi \to \mu^+\mu^-\right) = (5.961 \pm 0.033) \times 10^{-2}$ [55]. The branching fraction of the $\psi(2S)$ decay into two electrons is more precisely known than for the decay into two muons, and is therefore used with the assumption of lepton universality, neglecting the mass difference between muons and electrons. No systematic uncertainty is assigned for this assumption.

The absolute $\psi(2S)$ production cross-section is then derived from this ratio multiplied by the J/ψ production cross-section measured with less restrictive selection criteria on the muon particle identification, published in ref. [37],

$$\frac{\mathrm{d}^2\sigma_{\psi(2S)}}{\mathrm{d}p_{\mathrm{T}}\mathrm{d}y^*} = \frac{\mathrm{d}^2\sigma_{\psi(2S)}/\mathrm{d}p_{\mathrm{T}}\mathrm{d}y^*}{\mathrm{d}^2\sigma_{J/\psi}/\mathrm{d}p_{\mathrm{T}}\mathrm{d}y^*} \cdot \left[\frac{\mathrm{d}^2\sigma_{J/\psi}}{\mathrm{d}p_{\mathrm{T}}\mathrm{d}y^*}\right]_{\mathrm{pub}}. \tag{3.2}$$

Nuclear effects are quantified using the nuclear modification factor, $R_{p\mathrm{Pb}}$,

$$R_{p\mathrm{Pb}}(p_{\mathrm{T}}, y^*) \equiv \frac{1}{A}\frac{\mathrm{d}^2\sigma_{p\mathrm{Pb}}(p_{\mathrm{T}}, y^*)/\mathrm{d}p_{\mathrm{T}}\mathrm{d}y^*}{\mathrm{d}^2\sigma_{pp}(p_{\mathrm{T}}, y^*)/\mathrm{d}p_{\mathrm{T}}\mathrm{d}y^*}, \tag{3.3}$$

where $A = 208$ is the mass number of the Pb ion, $\mathrm{d}^2\sigma_{p\mathrm{Pb}}(p_{\mathrm{T}}, y^*)/\mathrm{d}p_{\mathrm{T}}\mathrm{d}y^*$ is the production cross-section in pPb or Pbp collisions and $\mathrm{d}^2\sigma_{pp}(p_{\mathrm{T}}, y^*)/\mathrm{d}p_{\mathrm{T}}\mathrm{d}y^*$ the reference production cross-section in pp collisions at the same centre-of-mass energy. In the absence of nuclear effects, the nuclear modification factor is equal to unity.

Similarly to the cross-section, the $\psi(2S)$ nuclear modification factor is derived from corrected yield ratios and the published J/ψ modification factor [56],

$$R_{p\mathrm{Pb}}^{\psi(2S)}(p_{\mathrm{T}}, y^*) = \frac{\left[\frac{\mathrm{d}^2\sigma_{\psi(2S)}/\mathrm{d}p_{\mathrm{T}}\mathrm{d}y^*}{\mathrm{d}^2\sigma_{J/\psi}/\mathrm{d}p_{\mathrm{T}}\mathrm{d}y^*}\right]_{p\mathrm{Pb}}}{\left[\frac{\mathrm{d}^2\sigma_{\psi(2S)}/\mathrm{d}p_{\mathrm{T}}\mathrm{d}y^*}{\mathrm{d}^2\sigma_{J/\psi}/\mathrm{d}p_{\mathrm{T}}\mathrm{d}y^*}\right]_{pp}} \cdot \left[R_{p\mathrm{Pb}}^{J/\psi}(p_{\mathrm{T}}, y^*)\right]_{\mathrm{pub}}. \tag{3.4}$$

The nuclear modification factor in Pbp collisions, $R_{\mathrm{Pb}p}^{\psi(2S)}(p_{\mathrm{T}}, y^*)$ is computed analogously. The reference $\psi(2S)$ to J/ψ cross-section ratio in pp collisions is obtained from measurements at 7 TeV by the LHCb collaboration [56] assuming that the ratio between $\psi(2S)$ and J/ψ

JHEP04(2024)111

production in a given $p_{\rm T}$ bin is the same at 7 TeV and at 8.16 TeV and is independent of the charmonium-state rapidity in the LHCb acceptance. This assumption is consistent with the results of the present analysis and with previous measurements [56]. No systematic uncertainty is assigned for this assumption.

The forward-to-backward ratios compare production in pPb and Pbp collisions in the common acceptance range $2.5 < |y^*| < 4.0$, without the need to know the reference cross-section in pp collisions. It is defined as

$$R_{\rm FB}(p_{\rm T}, y^*) = \frac{\left[\frac{{\rm d}\sigma(p_{\rm T}, y^*)}{{\rm d}p_{\rm T}}\right]_{p{\rm Pb}}}{\left[\frac{{\rm d}\sigma(p_{\rm T}, -y^*)}{{\rm d}p_{\rm T}}\right]_{{\rm Pb}p}}. \tag{3.5}$$

4 Event selection and cross-section determination

4.1 Selection

An online event selection is performed by a trigger system consisting of a hardware stage, which selects events containing at least one muon with $p_{\rm T}$ larger than 500 MeV/c, followed by a software stage. In the first stage of the software trigger, two muon tracks with $p_{\rm T} > 500\,{\rm MeV}/c$ are required to form a J/ψ or $\psi(2S)$ candidate with invariant mass $M_{\mu^+\mu^-} > 2.5\,{\rm GeV}/c^2$. In the second stage, J/ψ and $\psi(2S)$ candidates with an invariant mass within 120 MeV/c^2 of the known value of the J/ψ or $\psi(2S)$ mass [55] are selected.

At the analysis stage, each event is required to have at least one PV reconstructed from at least four tracks measured in the vertex detector. For events with multiple PVs, the PV that has the smallest $\chi^2_{\rm IP}$ with respect to the J/ψ or the $\psi(2S)$ candidate is chosen. Here, $\chi^2_{\rm IP}$ is defined as the difference between the vertex-fit χ^2 calculated with the J/ψ or $\psi(2S)$ meson candidate included in or excluded from the PV fit. Each identified muon track is required to be in the pseudorapidity range $2 < \eta < 5$, have a good-quality track fit, and have $p_{\rm T} > 750\,{\rm MeV}/c$ and $p_{\rm T} > 1000\,{\rm MeV}/c$ for J/ψ and $\psi(2S)$ candidates, respectively. The stricter selection for $\psi(2S)$ is due to a larger combinatorial background. The two muon tracks of the J/ψ or $\psi(2S)$ candidate must form a good-quality vertex.

4.2 Determination of signal yields

The reconstructed vertex of the J/ψ or $\psi(2S)$ mesons originating from b-hadron decays tends to be separated from the PV. This property is used to distinguish between prompt and nonprompt J/ψ or $\psi(2S)$ mesons by exploiting the pseudoproper time defined as

$$t_z \equiv \frac{(z - z_{\rm PV}) \times M}{p_z}, \tag{4.1}$$

where z and $z_{\rm PV}$ are the coordinates along the beam axis of the J/ψ or $\psi(2S)$ decay vertex and PV positions, p_z is the z component of the J/ψ or $\psi(2S)$ momentum and M the known J/ψ or $\psi(2S)$ mass. The yields of J/ψ and $\psi(2S)$ signals, for the prompt and nonprompt categories, are determined from a two-dimensional unbinned maximum-likelihood fit to their invariant-mass and pseudoproper-time distributions, performed independently for each $(p_{\rm T}, y^*)$ bin.

JHEP04(2024)111

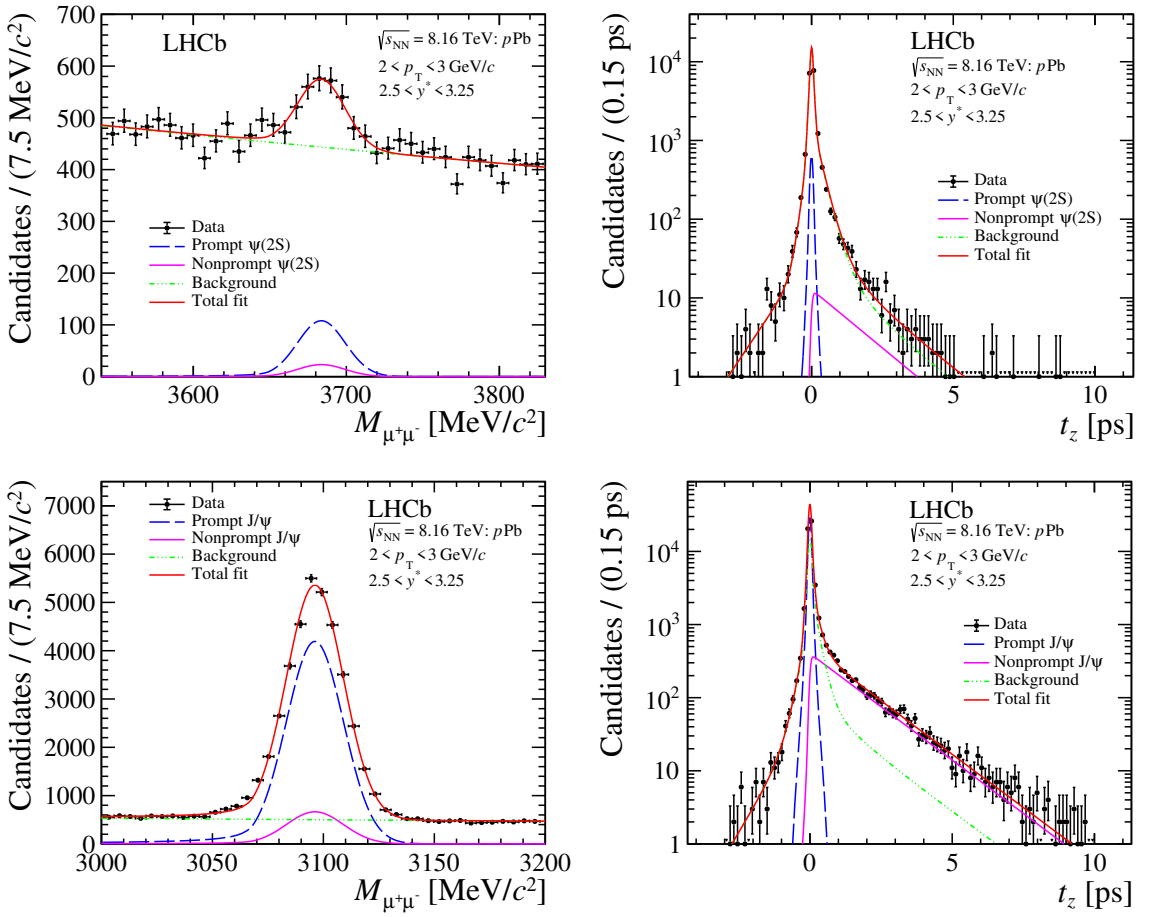

Figure 1. Distributions of (left) invariant mass and (right) pseudoproper time for (upper) $\psi(2S)$ and (lower) J/ψ candidates in the bin $2 < p_T < 3\,\text{GeV}/c$ and $2.5 < y^* < 3.25$. The data are overlaid with the fit results.

The invariant-mass distribution consists of two components: the J/ψ or $\psi(2S)$ signal and the background, which is only of combinatorial origin. In the fit function, the signal is described by a Crystal Ball function [57], and the combinatorial background by an exponential function. The t_z distribution of prompt J/ψ or $\psi(2S)$ is described by a Dirac δ-function $\delta(t_z)$, and that of nonprompt mesons by an exponential function. Both functions are convolved with a triple-Gaussian function to take into account the pseudoproper-time resolution. The background t_z distribution is described by an empirical function derived from the shape observed in the region $3200 < M_{\mu^+\mu^-} < 3250\,\text{MeV}/c^2$. This background is composed of muons from semileptonic decays of b and c hadrons and from decays of pions and kaons in the detector. The distribution is parameterised as a sum of a Dirac δ-function and of five exponential functions, three for positive t_z values and two for negative t_z values, convolved with the sum of two Gaussian functions. An example of the $\psi(2S)$ and J/ψ invariant mass and the pseudoproper-time distributions for one (p_T, y^*) bin is shown in figure 1 for the pPb sample, where the one-dimensional projections of the fit result are drawn on the distributions.

JHEP04(2024)111

4.3 Efficiencies

The total efficiency, ϵ_{tot}, is the product of the geometrical acceptance and the efficiencies for charged-track reconstruction, particle identification, and candidate and trigger selections. Samples of simulated events are used to evaluate these efficiencies except for the charged-track reconstruction and particle identification efficiencies, which are determined from calibration data samples. Inelastic pPb and Pbp collisions are simulated by the EPOS event generator, which is tuned to describe LHC data [58]. The $\psi(2S) \to \mu^+\mu^-$ and $J/\psi \to \mu^+\mu^-$ signal candidates are generated separately with the PYTHIA8 generator [59] in pp collisions with beams having momenta equal to the momenta per nucleon of the p and Pb beams. These events are merged with the EPOS collisions to build the samples out of which the efficiencies are computed. The decays of hadrons are simulated by EVTGEN [60], in which final-state electromagnetic radiation is modelled with PHOTOS [61]. The interaction of the particles with the detector, and the detector response, are implemented using the GEANT4 toolkit [62, 63] as described in ref. [64].

The charged-track reconstruction efficiency is first evaluated in simulation and is corrected per track using calibration samples. For this purpose, J/ψ candidates are formed with one fully reconstructed "tag" track and one "probe" track, reconstructed partially with a subset of the tracking sub-detectors and both tracks identified as muons [65], in data and in simulation. The tag-and-probe correction factors are extracted from pPb and Pbp data and J/ψ simulation samples, taking into account their dependence on the particle multiplicity. They are applied to the $\psi(2S)$ and J/ψ simulation in order to obtain the track reconstruction efficiencies in the $\psi(2S)$ and J/ψ p_{T} and y^* bins of the analysis.

The muon identification efficiency is determined for each track in data with a tag-and-probe method taking into account the efficiency variation as a function of track momentum, pseudorapidity and detector occupancy. Calibration samples of J/ψ mesons are selected by applying a tight identification criterion on one of the muons and no identification requirements on the second muon [66]. However, the calibration samples collected in pPb and Pbp collisions are limited in size. The efficiency is thus evaluated using the calibration samples collected in pp collisions, taking into account the differences in the detector occupancy between pp, pPb and Pbp collisions, which affects the muon identification performance. While the muon identification efficiency is observed to be robust against the variation of detector occupancies, the probability of hadron misidentification presents a stronger dependence on hit or track multiplicity. The $\psi(2S)$ and J/ψ simulation samples are assigned per-candidate weights according to the efficiencies determined per track in data. These weighted samples are used to compute the muon identification efficiency in bins of p_{T} and y^* of the $\psi(2S)$ or J/ψ meson.

The total efficiencies are found to be consistent for the prompt and nonprompt quarkonia. The ratio of the J/ψ and $\psi(2S)$ efficiencies is shown in figure 2 in each analysis bin, for pPb and Pbp collisions. The uncertainties include both statistical uncertainties and the systematic uncertainties described in the following section.

JHEP04(2024)111

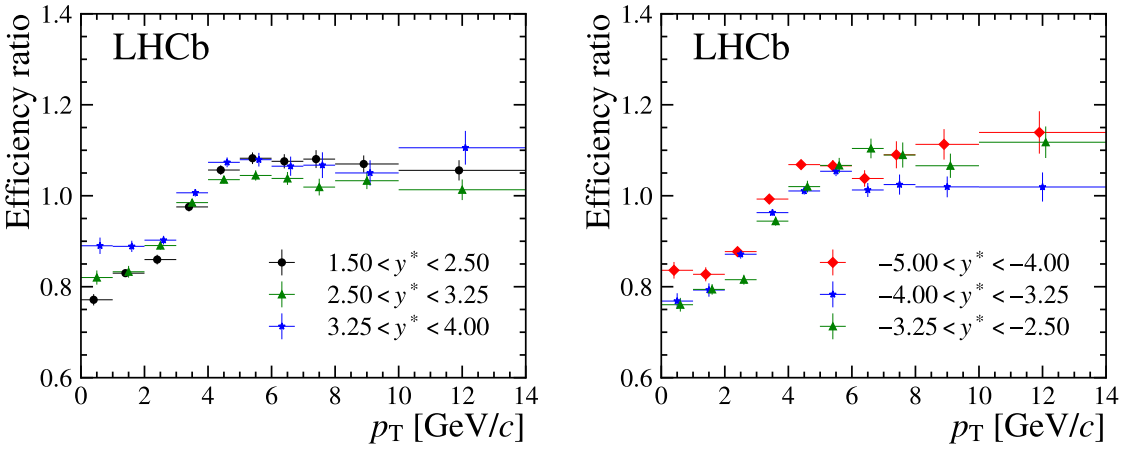

Figure 2. Ratio of J/ψ to $\psi(2S)$ total efficiencies as a function of the quarkonium p_T in different y^* intervals for (left) pPb and (right) Pbp collisions.

Source	pPb	Pbp
Signal extraction	2.2	2.2
Particle identification	0–1.7	0–2.0
Efficiency extrapolation at high multiplicity	5.0	5.0
Tracking	0–0.1	0–0.1
Hardware trigger	0–1.1	0–1.1
Particle multiplicity	5.0	5.0
Simulation sample size	0.3–3.2	0.4–4.0
$\frac{\mathcal{B}(J/\psi\to\mu^+\mu^-)}{\mathcal{B}(\psi(2S)\to\mu^+\mu^-)}$ (assuming lepton universality)	2.2	2.2

Table 1. Summary of relative systematic uncertainties in pPb and Pbp collisions on the ratio of $\psi(2S)$ to J/ψ cross-sections for prompt and nonprompt production. Uncertainties that are computed bin-by-bin are expressed as ranges from the minimum to maximum values. All uncertainties are assumed to be fully correlated between bins, apart from the uncertainty arising from the simulation sample size. Values are expressed as percentage.

5 Systematic uncertainties

The systematic uncertainties on the measurement of the cross-section ratio for prompt and nonprompt $\psi(2S)$ to J/ψ production are summarised in table 1. The efficiencies depend on the J/ψ and $\psi(2S)$ polarisation at production. Measurements by the ALICE and the LHCb collaborations in pp collisions [67–69] indicate a polarisation close to zero in the kinematic region covered in the analysis, with a negligible effect on the total detection efficiency. It is assumed that the $\psi(2S)$ and J/ψ mesons are also produced with no polarisation in the pPb and Pbp collisions. No systematic uncertainty is assigned to this assumption.

The $\psi(2S)$ and J/ψ meson yields are affected by the choice of the modelling of the signal mass shape in the fit. An uncertainty is evaluated using an alternative fit model where the

JHEP04(2024)111

signal mass shape is described by the sum of a Crystal Ball function and a Gaussian function. The relative difference of the signal yields between the two fits is 2.2%, which is assigned as a systematic uncertainty that is fully correlated between bins. The uncertainty associated with the choice of the shape of the t_z distribution is negligible.

The uncertainty on the muon identification efficiency has several contributions. The size of the calibration sample affects the statistical precision of the efficiency determined with the tag-and-probe method described in the previous section. The impact of the binning in muon momentum, pseudorapidity and detector occupancy used in that method is estimated by varying the binning scheme. Finally, an uncertainty due to the method used to determine the number of signal candidates in the calibration samples is also considered. The total systematic uncertainty due to these three sources varies between 0 and 2% and is assumed to be fully correlated between bins. The particle identification efficiency is determined from data control samples obtained from pp collisions [66]. The particle multiplicity in pPb collisions is larger than in pp collisions and the efficiencies in the high multiplicity bins are extrapolated from lower multiplicity values. The uncertainty associated with this procedure is estimated by comparing the J/ψ double-differential absolute cross-section obtained in this analysis with that published in ref. [37], which was obtained with looser selection requirements. They agree within 5%, which is taken as the uncertainty related to the particle identification efficiency extrapolation. The uncertainty related to charged track reconstruction, which largely cancels in the efficiency ratio, varies from 0 to 0.1% and is correlated between bins.

The hardware trigger efficiencies obtained from the simulation are validated by comparing them with the efficiencies measured in control samples in data [70]. A systematic uncertainty is evaluated by comparing the results in simulation and in data. This uncertainty varies between 0 and 1.1% and is assumed to be correlated between bins.

The reconstruction and PID efficiencies depend on the particle multiplicity. The observed particle multiplicity distributions are compatible between events with $\psi(2S)$ and J/ψ mesons, however the uncertainties are large. Since these distributions could be different [71], efficiencies are recomputed varying the multiplicity distributions between $\psi(2S)$ and J/ψ events within their statistical uncertainties. Variations of 5% are observed and this is assigned as the systematic uncertainty related to possible different multiplicity distributions in events with J/ψ or $\psi(2S)$ candidates. The finite size of the simulation sample used for the efficiency determination introduces a systematic uncertainty, which varies between 0.3% and 4.0%. The uncertainty on the ratio of branching fractions is 2.2%.

The systematic uncertainties are assumed to be uncorrelated between the cross-section ratios and the J/ψ cross-section measurement in ref. [56] when computing the $\psi(2S)$ cross-sections. They are also assumed to uncorrelated with the ratio of reference cross-sections in pp collisions at 8.16 TeV used to compute the modification factors and their ratios.

6 Results

6.1 Ratios of $\psi(2S)$ to J/ψ cross-sections

The prompt production cross-section ratios, $\frac{\sigma_{\psi(2S)}}{\sigma_{J/\psi}}$, are shown in figure 3 as a function of p_{T} in the three rapidity intervals of the analysis of pPb and Pbp collisions. All numerical

JHEP04(2024)111

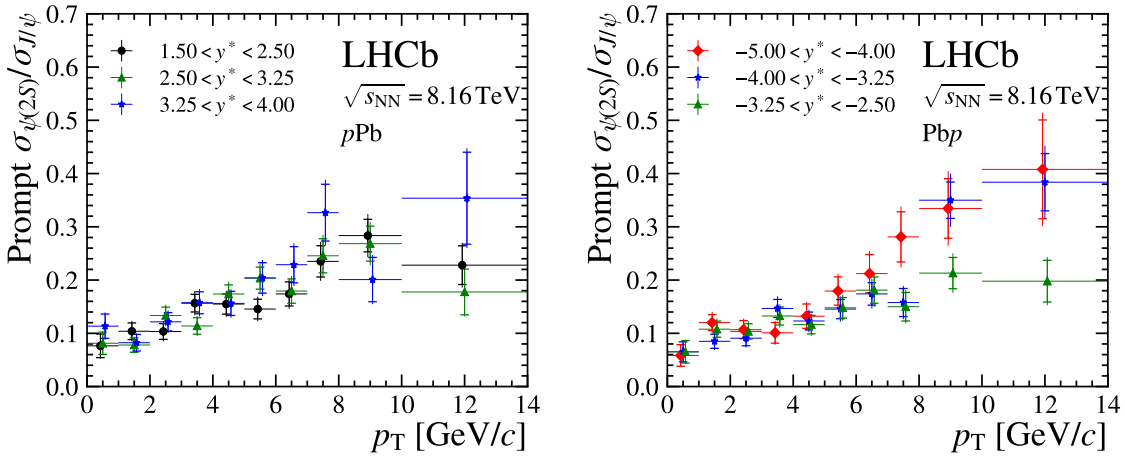

Figure 3. Ratio of prompt $\psi(2S)$ to prompt J/ψ production cross-section in (left) pPb and (right) Pbp collisions, as a function of p_T for the different rapidity intervals. Horizontal error bars are the bin widths, vertical error bars represent the statistical and total uncertainties.

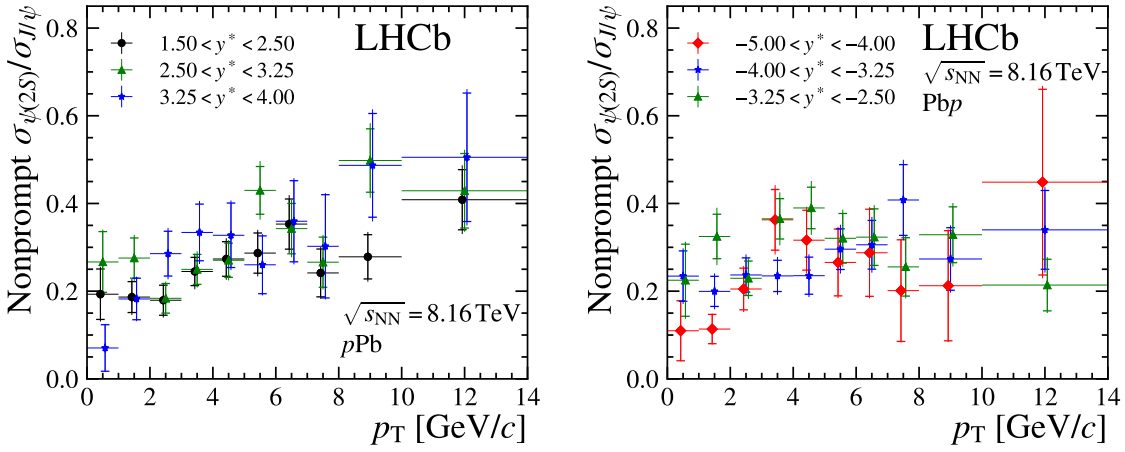

Figure 4. Ratio of nonprompt $\psi(2S)$ to nonprompt J/ψ production cross-section in (left) pPb and (right) Pbp collisions, as a function of p_T for the different rapidity intervals. Horizontal error bars are the bin widths, vertical error bars represent the statistical and total uncertainties.

values corresponding to the figures are available in the appendices A – E. The production cross-section ratios for the nonprompt production are shown in figure 4.

The prompt production cross-section ratios as a function of p_T, integrated in the range $1.5 < y^* < 4.0$ for pPb collisions and $-5.0 < y^* < -2.5$ for Pbp collisions, are shown in figure 5. The corresponding values for nonprompt production are shown in figure 6. The production cross-section ratios are also extracted as a function of rapidity integrated in the range $0 < p_T < 14\,\text{GeV}/c$. They are shown in figure 7.

JHEP04(2024)111

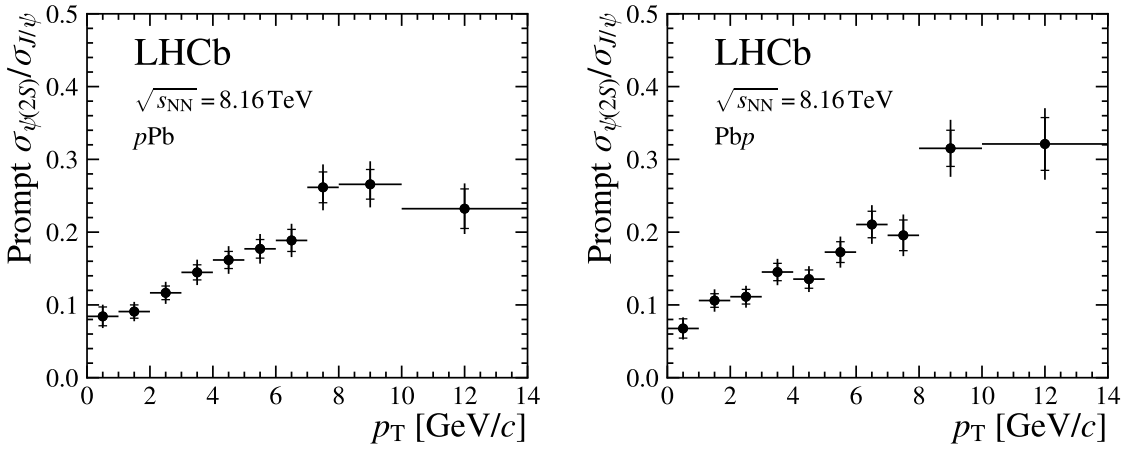

Figure 5. Ratio of prompt $\psi(2S)$ to prompt J/ψ production cross-sections in (left) pPb collisions, integrated over $1.5 < y^* < 4.0$, and (right) Pbp collisions, integrated over $-5.0 < y^* < -2.5$, as a function of p_T. Horizontal error bars are the bin widths, vertical error bars represent the statistical and total uncertainties.

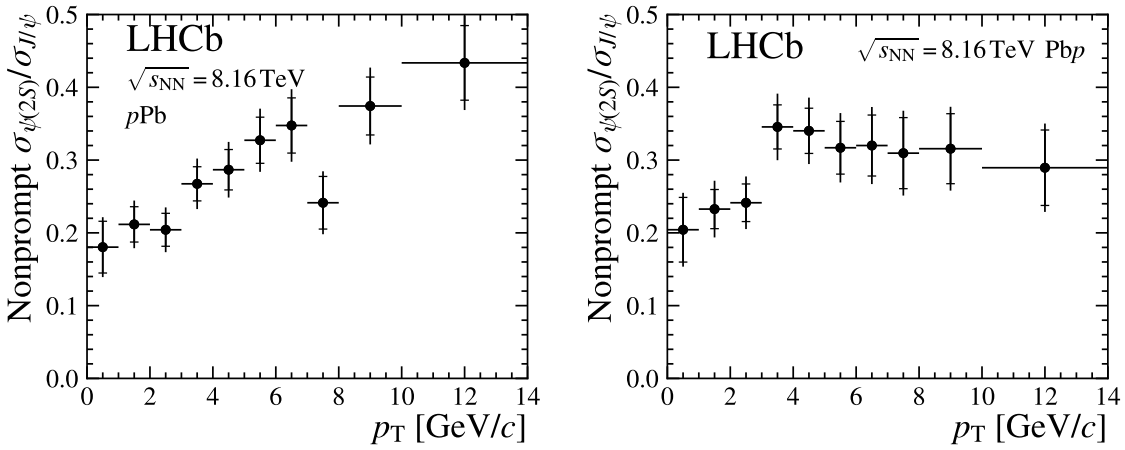

Figure 6. Ratio of nonprompt $\psi(2S)$ to nonprompt J/ψ production cross-section in (left) pPb collisions, integrated over $1.5 < y^* < 4.0$, and (right) Pbp collisions, integrated over $-5.0 < y^* < -2.5$, as a function of p_T. Horizontal error bars are the bin widths, vertical error bars represent the statistical and total uncertainties.

6.2 Cross-sections for $\psi(2S)$ production

The absolute $\psi(2S)$ cross-sections are obtained multiplying the ratios shown in the previous section by the measured values of the J/ψ cross-sections [37], in the same p_T and y^* bins. The prompt $\psi(2S)$ production cross-section is shown in figure 8 and the nonprompt cross-section in figure 9, as a function of p_T for different rapidity intervals, for pPb and Pbp collisions. The cross-sections, integrated over y^* in the LHCb acceptance and as a function of p_T are shown in figure 10.

JHEP04(2024)111

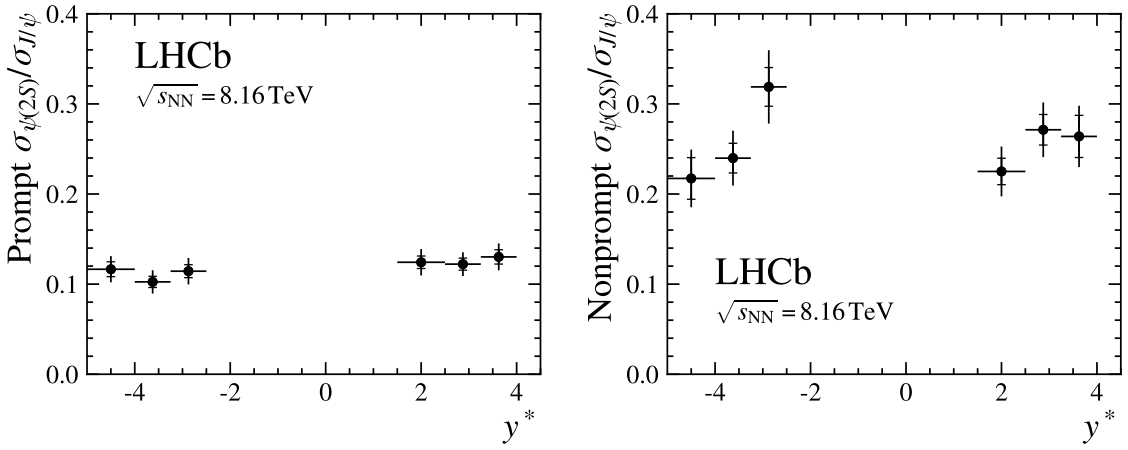

Figure 7. Ratio of (left) prompt and (right) nonprompt $\psi(2S)$ to J/ψ production cross-section, as a function of rapidity, integrated over p_T. Horizontal error bars are the bin widths, vertical error bars represent the statistical and total uncertainties.

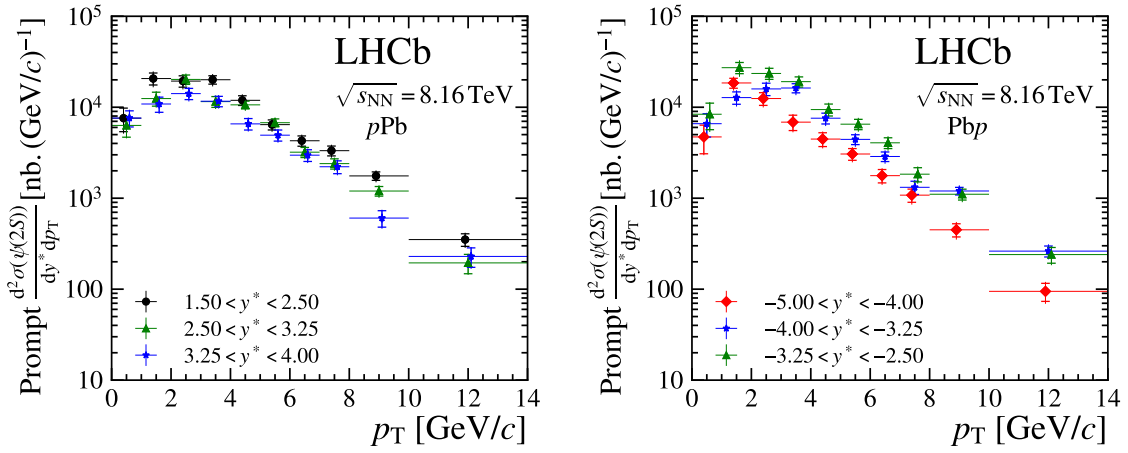

Figure 8. Absolute prompt $\psi(2S)$ production cross-section in (left) pPb and (right) Pbp collisions, as a function of p_T for the different rapidity intervals. Horizontal error bars are the bin widths, vertical error bars represent the statistical and total uncertainties.

6.3 Nuclear modification factors for $\psi(2S)$ production

The $\psi(2S)$ nuclear modification factors integrated over y^* as a function of p_T are shown in figure 11. The kinematic dependence of the prompt $\psi(2S)$ nuclear modification factor is similar to that of the J/ψ meson seen in ref. [37], with additional suppression. The nonprompt $\psi(2S)$ nuclear modification factor is consistent with the J/ψ one [37] with larger uncertainties due to the smaller sample size.

6.4 Forward-to-backward ratio for $\psi(2S)$ production

The $\psi(2S)$ forward-to-backward ratios for prompt and nonprompt $\psi(2S)$ production integrated over y^* as a function of p_T and integrated over p_T as a function of y^* are shown in figure 12.

JHEP04(2024)111

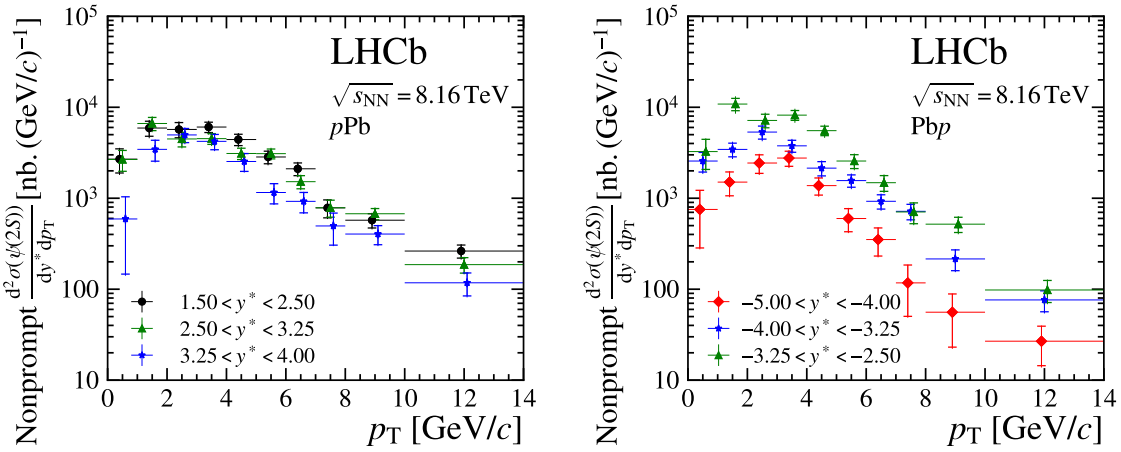

Figure 9. Absolute nonprompt $\psi(2S)$ production cross-section in (left) pPb and (right) Pbp collisions, as a function of $p_{\rm T}$ for the different rapidity intervals. Horizontal error bars are the bin widths, vertical error bars represent the statistical and total uncertainties.

JHEP04(2024)111

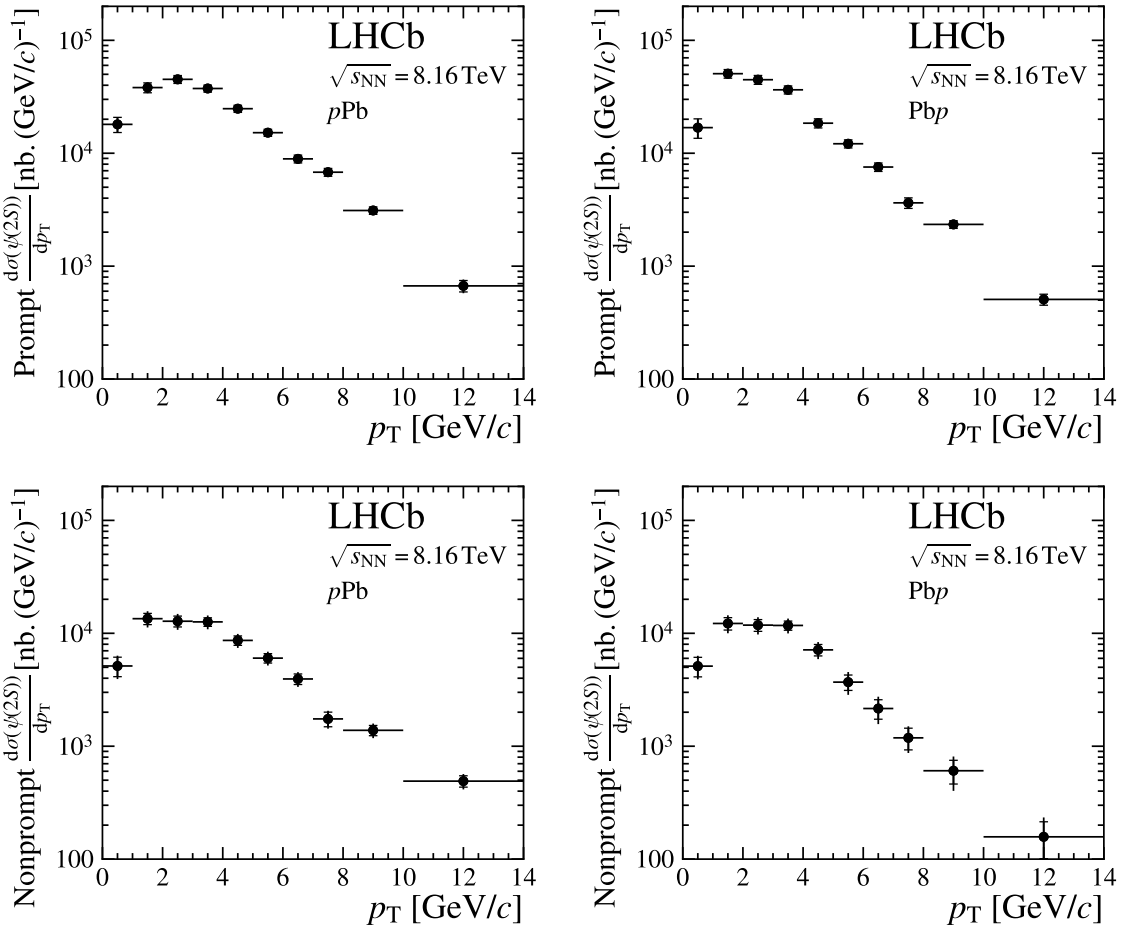

Figure 10. Absolute production cross-section as a function of $p_{\rm T}$ for (top left) prompt $\psi(2S)$ in pPb collisions, integrated over $1.5 < y^* < 4.0$, (top right) prompt $\psi(2S)$ in Pbp collisions, integrated over $-5.0 < y^* < -2.5$, (bottom left) nonprompt $\psi(2S)$ in pPb collisions, integrated over $1.5 < y^* < 4.0$, (bottom right) nonprompt $\psi(2S)$ in Pbp collisions, integrated over $-5.0 < y^* < -2.5$. Horizontal error bars are the bin widths, vertical error bars represent the statistical and total uncertainties.

JHEP04(2024)111

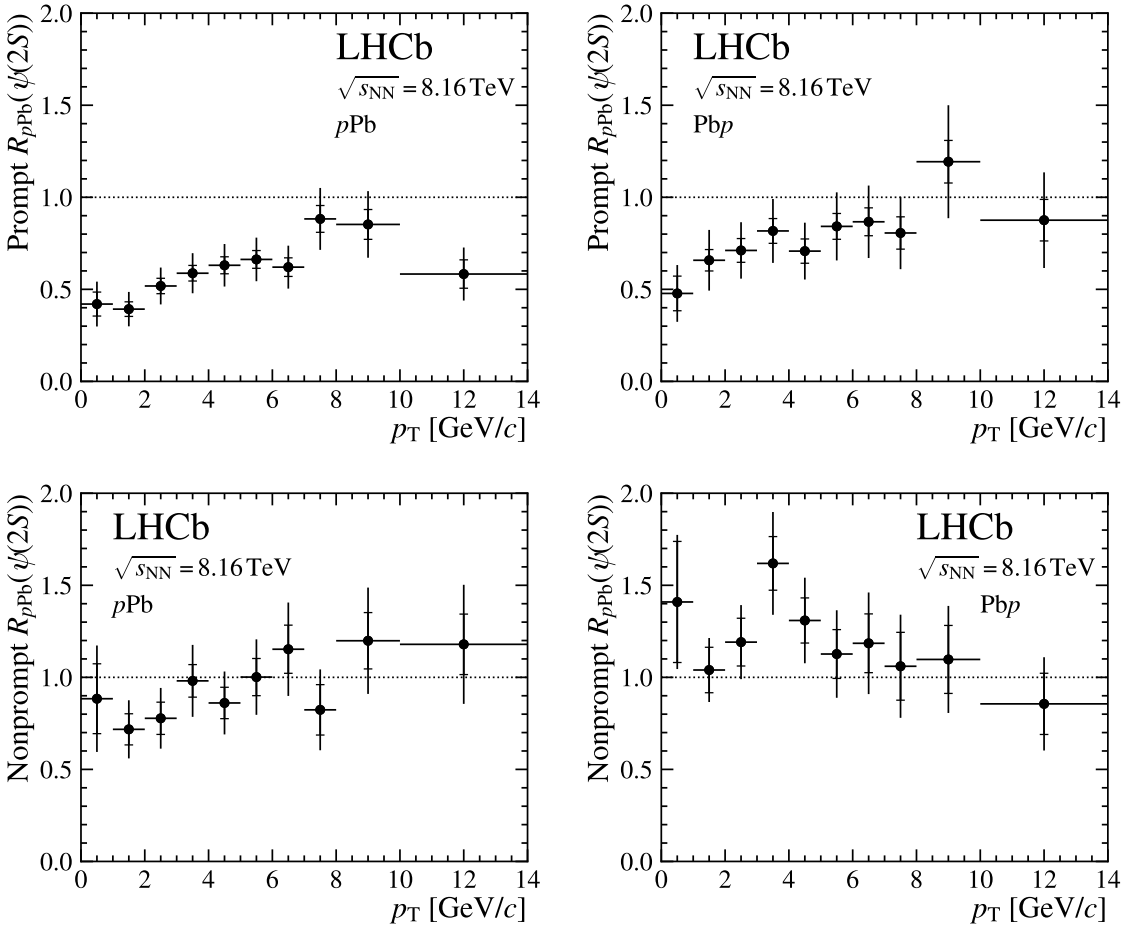

Figure 11. Nuclear modification factor as a function of $p_{\rm T}$, for (top left) prompt $\psi(2S)$ in pPb collisions, integrated over $1.5 < y^* < 4.0$, (top right) prompt $\psi(2S)$ in Pbp collisions, integrated over $-5.0 < y^* < -2.5$, (bottom left) nonprompt $\psi(2S)$ in pPb collisions, integrated over $1.5 < y^* < 4.0$, and (bottom right) nonprompt $\psi(2S)$ in Pbp collisions, integrated over $-5.0 < y^* < -2.5$. Horizontal error bars are the bin widths, vertical error bars represent the statistical and total uncertainties.

JHEP04(2024)111

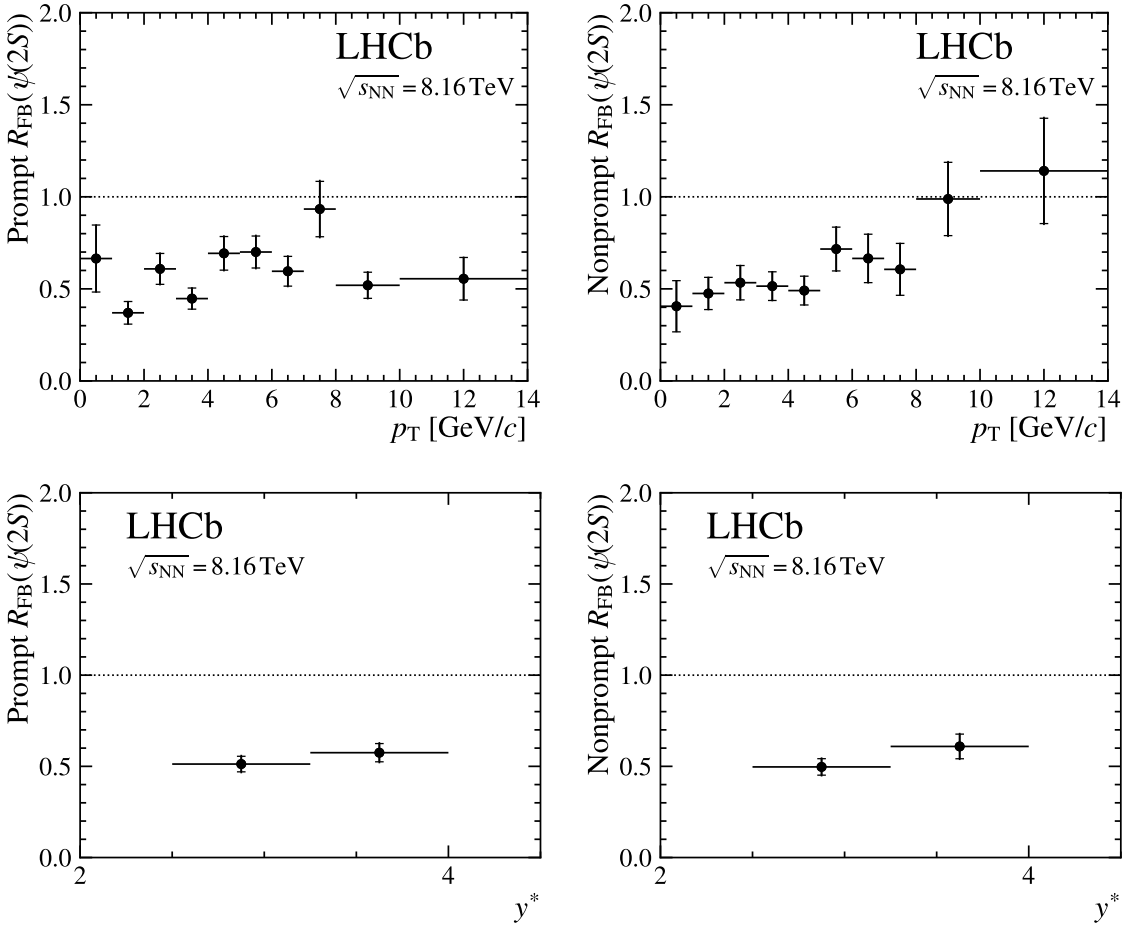

Figure 12. Forward-to-backward ratio as a function of $p_{\rm T}$ and integrated over $2.5 < |y^*| < 4.0$ for (top left) prompt and (top right) nonprompt $\psi(2S)$; as a function of y^* and integrated over $p_{\rm T}$ for (bottom left) prompt and (bottom right) nonprompt $\psi(2S)$ as a function of $p_{\rm T}$. Horizontal error bars are the bin widths, vertical error bars represent the statistical and total uncertainties.

JHEP04(2024)111

6.5 Double cross-section ratios

In this section, several predictions of phenomenological approaches are compared with the experimental data. These comparisons use ratios of nuclear modification factors, "cross-section double ratios", since many sources of uncertainty, both theoretical and experimental, cancel out to a large extent. The double ratios are defined as

$$R^{p\mathrm{Pb}}_{\psi(2S)/J/\psi} = \frac{R_{p\mathrm{Pb}}(\psi(2S))}{R_{p\mathrm{Pb}}(J/\psi)} = \frac{\left[\frac{\sigma(\psi(2S))}{\sigma(J/\psi)}\right]_{p\mathrm{Pb}}}{\left[\frac{\sigma(\psi(2S))}{\sigma(J/\psi)}\right]_{pp}}. \tag{6.1}$$

The value of this ratio is expected to be equal to one in the case of nonprompt production since the modifications of the production due to the medium affect only the b-hadron production and not the final $\psi(2S)$ or J/ψ states. It should also be equal to one if the production of the $\psi(2S)$ and J/ψ in proton-lead collisions is only modified by initial-state effects and not final-state effects.

Their values as a function of p_{T} and integrated over y^* for prompt and nonprompt production are shown in figure 13 and as a function of rapidity and integrated over p_{T} in figure 14. The ratio integrated over p_{T} is shown in figure 15. It is compared with the measurement at $\sqrt{s_{\mathrm{NN}}} = 5\,\mathrm{TeV}$ [45]. The results obtained at 8.16 TeV are more precise than those at 5 TeV; they are compatible with each other within uncertainties.

The double-ratio results for nonprompt production are compatible with unity as expected. The results for prompt production indicate a larger suppression of the excited $\psi(2S)$ state compared to the J/ψ state. This confirms earlier, similar results obtained at 5 TeV by the ALICE [40], CMS [44] and LHCb [45] collaborations, at 8.16 TeV by the ALICE collaboration [42] and at 200 GeV by the PHENIX collaboration [39]. This phenomenon is not explained with the phenomenological models used for the description of J/ψ production. They assume that the nuclear suppression of the quarkonium state is induced at a timescale shorter than the hadronisation timescale. It follows that the mechanisms should apply universally to the J/ψ and $\psi(2S)$ states. Due to the proximity of the J/ψ and $\psi(2S)$ masses, the nuclear effects are expected to be the same for the two mesons. These considerations apply to all main classes of modification models usually considered: nPDF modifications [28, 72, 73], the standard CGC framework [29, 30] or coherent energy loss [25].

A good understanding of the suppression of $\psi(2S)$ over J/ψ production is crucial for the interpretation of measurements in heavy-ion collisions such as in PbPb collisions at the LHC. In PbPb collisions, the previously mentioned models predict different behaviours of the $\psi(2S)$ to J/ψ cross-section ratio in the presence of a deconfined phase. Therefore, the measurement of this production ratio in pPb or Pbp collisions, where a deconfined system is not expected to be created, provides important inputs to the models to describe the charmonium behaviour in heavy-ion collisions.

The modification of prompt $\psi(2S)$ production compared to that of the J/ψ in pPb or Pbp collisions can be caused by interactions at late stages of the collision that do not obey simple QCD factorisation. There are different models exploiting this idea:

- The Comover model [46]: according to the observed final-state particle density, it assumes an interaction cross-section between the quarkonium and a "comoving" medium,

JHEP04(2024)111

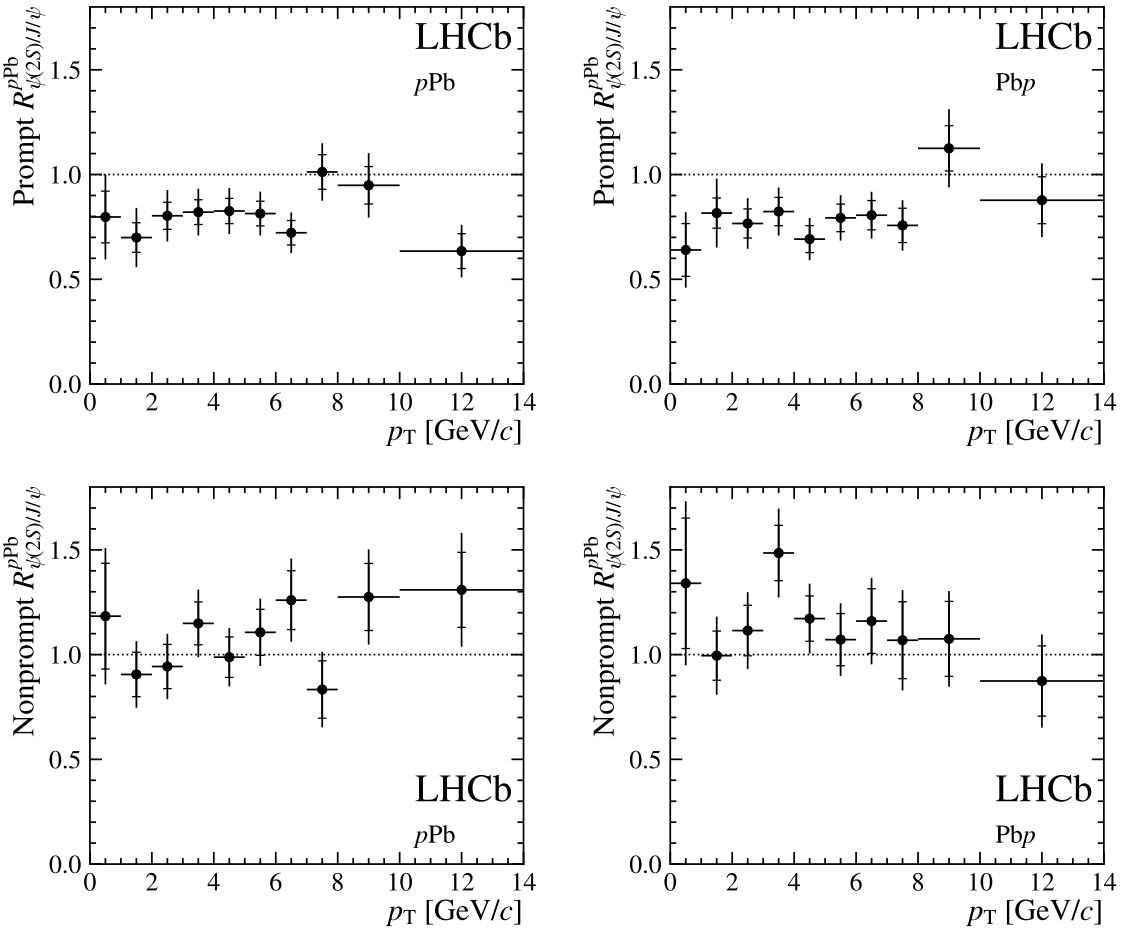

Figure 13. Cross-section double ratios $R^{pPb}_{\psi(2S)/J/\psi}$ as a function of p_T for (top left) prompt production in pPb collisions, integrated over $1.5 < y^* < 4.0$, (top right) prompt production in Pbp collisions, integrated over $-5.0 < y^* < -2.5$, (bottom left) nonprompt production in pPb collisions, integrated over $1.5 < y^* < 4.0$, (bottom right) nonprompt production in Pbp collisions, integrated over $-5.0 < y^* < -2.5$. Horizontal error bars are the bin widths, vertical error bars represent the statistical and total uncertainties.

composed of particles travelling along with the $c\bar{c}$ quark pair. This cross-section depends on the size, hence binding enery, of the quarkonium state, *i.e.* is larger for the $\psi(2S)$ excited state than for the J/ψ ground state.

- A combined CGC and improved Color Evaporation Model (GCG+ICEM) [47]: the short distance production of the charm and anti-charm pair is described by the standard CGC model, while the hadronisation into the J/ψ or $\psi(2S)$ states is computed with the ICEM. The effects breaking factorisation in the hadronisation are due to additional parton comovers. They are modelled with a cutoff parameter Λ that represents the average gluon p_T kick.

Figure 16 (left) shows the comparison between the data and the CGC+ICEM model [47] with two different values of Λ, 10 MeV and 20 MeV, as a function of p_T in the pPb configuration

JHEP04(2024)111

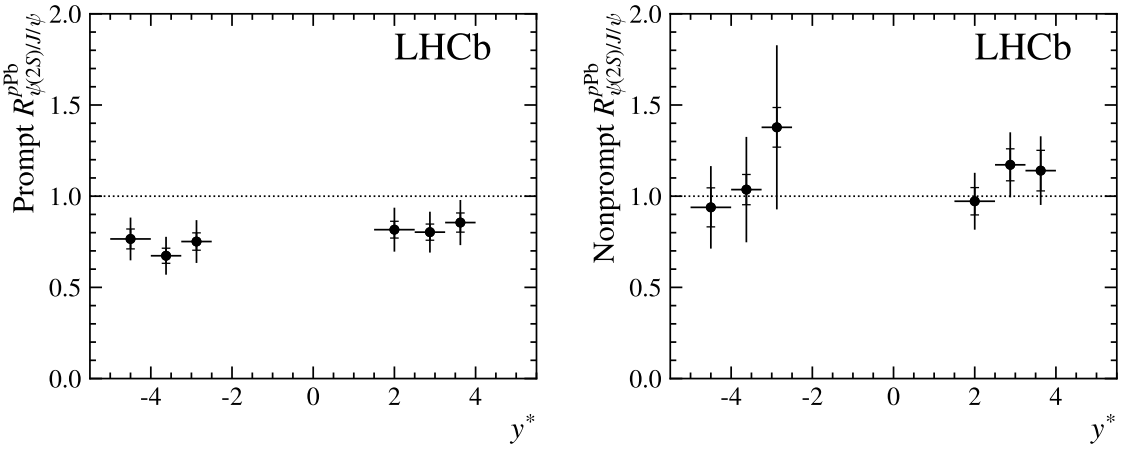

Figure 14. Cross-section double ratios $R^{pPb}_{\psi(2S)/J/\psi}$ as a function of y^*, for (left) prompt and (right) nonprompt production. Horizontal error bars are the bin widths, vertical error bars represent the statistical and total uncertainties.

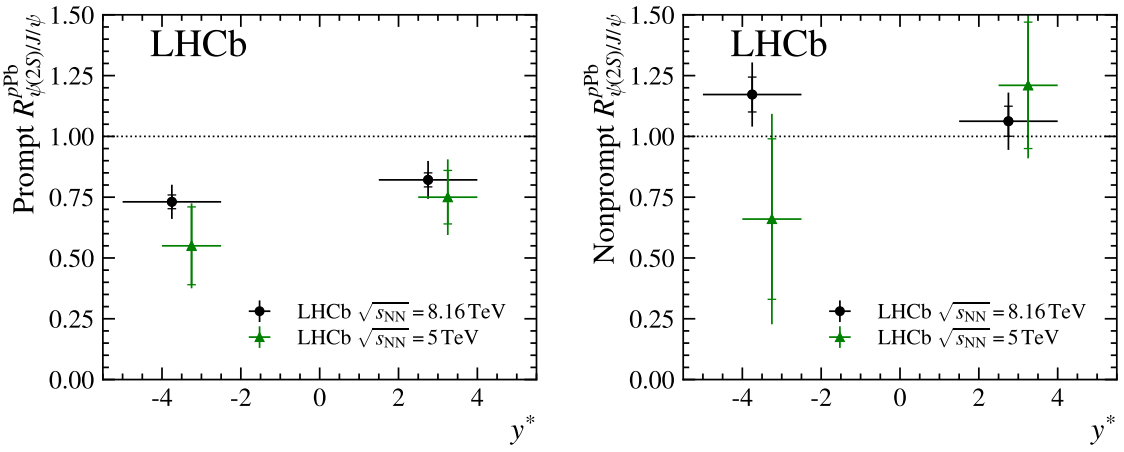

Figure 15. Cross-section double ratios $R^{pPb}_{\psi(2S)/J/\psi}$ as a function of y^*, for (left) prompt and (right) nonprompt production. The green triangles with error bars correspond to the LHCb measurement at 5 TeV [45]. Horizontal error bars are the bin widths, vertical error bars represent the statistical and total uncertainties.

for prompt production. Figure 16 (right) shows, in addition, the comparison with the Comover model [46], as a function of y^*. The models can describe the data reasonably well with appropriate parameter choices that also describe RHIC data at lower collision energy [46, 47]. Due to the feed-down of $\psi(2S)$ decays contributing to the J/ψ production, the difference in nuclear modification between the two states implies an effect on the J/ψ production which is not included in the computations. However, given the small contribution of the $\psi(2S)$ feed-down decays (10 to 20%), and the additional observed suppression of 25%, these effects are below the size of the data uncertainties.

JHEP04(2024)111

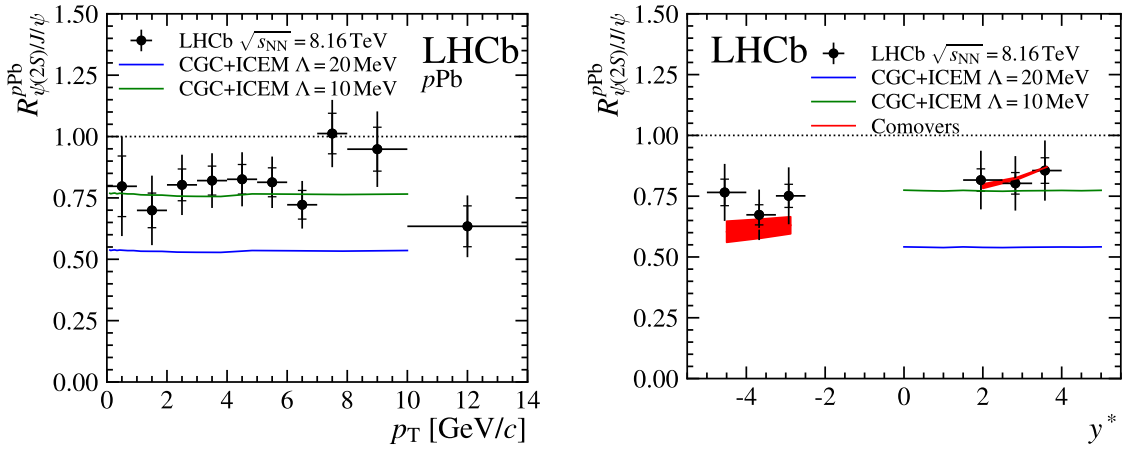

Figure 16. Prompt cross-section double ratios $R^{pPb}_{\psi(2S)/J/\psi}$ (left) as a function of p_T and integrated over $1.5 < y^* < 4.0$, and (right) as a function of y^* and integrated over p_T, compared with a CGC soft gluon interaction model with a scale (green) $\Lambda = 10\,\text{MeV}$ and (blue) $\Lambda = 20\,\text{MeV}$ and a (red) comover model (only for the y^* dependence). Horizontal error bars are the bin widths, vertical error bars the statistical and total uncertainties.

7 Conclusion

The measurement of $\psi(2S)$ production in pPb and Pbp collisions at $\sqrt{s_{NN}} = 8.16\,\text{TeV}$ is presented and is compared with J/ψ production in the same collision system and with the production in pp collisions, at the same center-of-mass energy. The ratio of prompt $\psi(2S)$ and J/ψ modification factors, $R_{p\text{Pb}}(\psi(2S))/R_{p\text{Pb}}(J/\psi)$, is measured to be below unity, indicating factorisation breaking with respect to the final state. The ratio of nonprompt $\psi(2S)$ and J/ψ modification factors is compatible with one, as expected since the nuclear effects affect b-hadron production but not their decays. These findings are supported by the corresponding measurements of the nuclear modification factor. This additional suppression seen in prompt $\psi(2S)$ production is compatible between the forward (pPb collisions) and backward (Pbp collisions) rapidity ranges and amounts to approximately 25% in the modification factor ratio integrated over p_T. With increasing p_T, the suppression tends to be smaller although large statistical uncertainties at high p_T prevent firm statements. The observed behaviour can be described by models featuring late-stage interactions breaking preferentially $\psi(2S)$ mesons compared to J/ψ mesons. These findings are important to constrain factorisation breaking with respect to the final state in nuclear collisions in order to interpret quarkonium data in heavy-ion collisions.

Acknowledgments

We express our gratitude to our colleagues in the CERN accelerator departments for the excellent performance of the LHC. We thank the technical and administrative staff at the LHCb institutes. We acknowledge support from CERN and from the national agencies: CAPES, CNPq, FAPERJ and FINEP (Brazil); MOST and NSFC (China); CNRS/IN2P3

JHEP04(2024)111

(France); BMBF, DFG and MPG (Germany); INFN (Italy); NWO (Netherlands); MNiSW and NCN (Poland); MCID/IFA (Romania); MICINN (Spain); SNSF and SER (Switzerland); NASU (Ukraine); STFC (United Kingdom); DOE NP and NSF (U.S.A.). We acknowledge the computing resources that are provided by CERN, IN2P3 (France), KIT and DESY (Germany), INFN (Italy), SURF (Netherlands), PIC (Spain), GridPP (United Kingdom), CSCS (Switzerland), IFIN-HH (Romania), CBPF (Brazil), and Polish WLCG (Poland). We are indebted to the communities behind the multiple open-source software packages on which we depend. Individual groups or members have received support from ARC and ARDC (Australia); Key Research Program of Frontier Sciences of CAS, CAS PIFI, CAS CCEPP, Fundamental Research Funds for the Central Universities, and Sci. & Tech. Program of Guangzhou (China); Minciencias (Colombia); EPLANET, Marie Skłodowska-Curie Actions, ERC and NextGenerationEU (European Union); A*MIDEX, ANR, IPhU and Labex P2IO, and Région Auvergne-Rhône-Alpes (France); AvH Foundation (Germany); ICSC (Italy); GVA, XuntaGal, GENCAT, Inditex, InTalent and Prog. Atracción Talento, CM (Spain); SRC (Sweden); the Leverhulme Trust, the Royal Society and UKRI (United Kingdom).

Tables with numerical results. The tables in the following appendices show the numerical values corresponding to the figures presenting the measurements. The cross-section ratios of $\psi(2S)$ over J/ψ, in bins of p_{T} and y^*, are given in table 2 for prompt production in pPb collisions and table 3 in Pbp collisions. The same ratios for nonprompt production are in table 4 in pPb collisions and in table 5 in Pbp collisions. These ratios integrated over y^*, in bins of p_{T} are shown in table 6 for pPb collisions and table 7 for Pbp collisions for prompt production, and in table 8 and table 9 for Pbp collisions. The ratios integrated over p_{T}, in bins of y^* are given in table 10 for prompt production and table 11 for nonprompt production.

The asbolute $\psi(2S)$ cross-sections in bins of p_{T} and y^* are available in table 12 for pPb collisions and table 13 for Pbp collisions, for prompt production, and in table 14 for pPb collisions and table 15 for Pbp collisions for nonprompt production. The values integrated over y^*, in bins of p_{T}, are in table 16 for prompt production in pPb collisions and in table 17 in Pbp collisions; the values for nonprompt production are in table 18 for pPb collisions and in table 19 Pbp collisions.

The $\psi(2S)$ nuclear modification factors in bins of p_{T}, integrated over y^*, are given in table 20 for prompt production in pPb collisions, in table 21 for prompt production in Pbp collisions, in table 22 for nonprompt production in pPb collisions and table 23 for nonprompt production in Pbp collisions. The $\psi(2S)$ forward-to-backward ratios are shown, in bins of p_{T} integrated over y^*, in table 24 for prompt production and in table 25 for nonprompt production. They are also given in bins of y^* integrated over p_{T} in table 26 for prompt production and in table 27 for nonprompt production.

The $\psi(2S)$ to J/ψ double cross-section ratios are shown in bins of p_{T}, integrated over y^*, in table 28 for prompt production in pPb collisions, in table 29 for prompt production in pPb collisions, in table 30 for prompt production in pPb collisions and in table 31 for nonprompt production in Pbp collisions. The values in bins of y^*, integrated over p_{T}, are given in table 32 for prompt production and in table 33 for nonprompt production. Finally, the ratios integrated over p_{T} and y^* are given in table 34 for prompt production and in table 35 for nonprompt production.

JHEP04(2024)111

A Cross-section ratios

p_{T} interval (GeV/c)	y^* interval	$\sigma_{\psi(2S)}/\sigma_{J/\psi}$
$0 < p_{\mathrm{T}} < 1$	$1.50 < y^* < 2.50$	$0.08 \pm 0.02 \pm 0.01$
$0 < p_{\mathrm{T}} < 1$	$2.50 < y^* < 3.25$	$0.08 \pm 0.02 \pm 0.01$
$0 < p_{\mathrm{T}} < 1$	$3.25 < y^* < 4.00$	$0.11 \pm 0.02 \pm 0.01$
$1 < p_{\mathrm{T}} < 2$	$1.50 < y^* < 2.50$	$0.10 \pm 0.02 \pm 0.01$
$1 < p_{\mathrm{T}} < 2$	$2.50 < y^* < 3.25$	$0.08 \pm 0.01 \pm 0.01$
$1 < p_{\mathrm{T}} < 2$	$3.25 < y^* < 4.00$	$0.08 \pm 0.02 \pm 0.01$
$2 < p_{\mathrm{T}} < 3$	$1.50 < y^* < 2.50$	$0.10 \pm 0.01 \pm 0.01$
$2 < p_{\mathrm{T}} < 3$	$2.50 < y^* < 3.25$	$0.13 \pm 0.02 \pm 0.01$
$2 < p_{\mathrm{T}} < 3$	$3.25 < y^* < 4.00$	$0.12 \pm 0.02 \pm 0.01$
$3 < p_{\mathrm{T}} < 4$	$1.50 < y^* < 2.50$	$0.16 \pm 0.02 \pm 0.02$
$3 < p_{\mathrm{T}} < 4$	$2.50 < y^* < 3.25$	$0.11 \pm 0.02 \pm 0.01$
$3 < p_{\mathrm{T}} < 4$	$3.25 < y^* < 4.00$	$0.16 \pm 0.02 \pm 0.01$
$4 < p_{\mathrm{T}} < 5$	$1.50 < y^* < 2.50$	$0.15 \pm 0.02 \pm 0.01$
$4 < p_{\mathrm{T}} < 5$	$2.50 < y^* < 3.25$	$0.17 \pm 0.02 \pm 0.02$
$4 < p_{\mathrm{T}} < 5$	$3.25 < y^* < 4.00$	$0.16 \pm 0.02 \pm 0.01$
$5 < p_{\mathrm{T}} < 6$	$1.50 < y^* < 2.50$	$0.15 \pm 0.02 \pm 0.01$
$5 < p_{\mathrm{T}} < 6$	$2.50 < y^* < 3.25$	$0.20 \pm 0.02 \pm 0.02$
$5 < p_{\mathrm{T}} < 6$	$3.25 < y^* < 4.00$	$0.20 \pm 0.03 \pm 0.02$
$6 < p_{\mathrm{T}} < 7$	$1.50 < y^* < 2.50$	$0.17 \pm 0.02 \pm 0.02$
$6 < p_{\mathrm{T}} < 7$	$2.50 < y^* < 3.25$	$0.18 \pm 0.02 \pm 0.02$
$6 < p_{\mathrm{T}} < 7$	$3.25 < y^* < 4.00$	$0.23 \pm 0.03 \pm 0.02$
$7 < p_{\mathrm{T}} < 8$	$1.50 < y^* < 2.50$	$0.24 \pm 0.03 \pm 0.02$
$7 < p_{\mathrm{T}} < 8$	$2.50 < y^* < 3.25$	$0.25 \pm 0.03 \pm 0.02$
$7 < p_{\mathrm{T}} < 8$	$3.25 < y^* < 4.00$	$0.33 \pm 0.05 \pm 0.03$
$8 < p_{\mathrm{T}} < 10$	$1.50 < y^* < 2.50$	$0.28 \pm 0.03 \pm 0.03$
$8 < p_{\mathrm{T}} < 10$	$2.50 < y^* < 3.25$	$0.27 \pm 0.03 \pm 0.02$
$8 < p_{\mathrm{T}} < 10$	$3.25 < y^* < 4.00$	$0.20 \pm 0.04 \pm 0.02$
$10 < p_{\mathrm{T}} < 14$	$1.50 < y^* < 2.50$	$0.23 \pm 0.04 \pm 0.02$
$10 < p_{\mathrm{T}} < 14$	$2.50 < y^* < 3.25$	$0.18 \pm 0.04 \pm 0.02$
$10 < p_{\mathrm{T}} < 14$	$3.25 < y^* < 4.00$	$0.35 \pm 0.09 \pm 0.04$

Table 2. Cross-section ratios of $\psi(2S)$ over J/ψ prompt production in pPb collisions. The first uncertainty is statistical and the second systematic.

JHEP04(2024)111

p_{T} interval (GeV/c)	y^* interval	$\sigma_{\psi(2S)}/\sigma_{J/\psi}$
$0 < p_{\mathrm{T}} < 1$	$-3.25 < y^* < -2.50$	$0.07 \pm 0.02 \pm 0.01$
$0 < p_{\mathrm{T}} < 1$	$-4.00 < y^* < -3.25$	$0.07 \pm 0.02 \pm 0.01$
$0 < p_{\mathrm{T}} < 1$	$-5.00 < y^* < -4.00$	$0.06 \pm 0.02 \pm 0.01$
$1 < p_{\mathrm{T}} < 2$	$-3.25 < y^* < -2.50$	$0.11 \pm 0.02 \pm 0.01$
$1 < p_{\mathrm{T}} < 2$	$-4.00 < y^* < -3.25$	$0.09 \pm 0.01 \pm 0.01$
$1 < p_{\mathrm{T}} < 2$	$-5.00 < y^* < -4.00$	$0.12 \pm 0.02 \pm 0.01$
$2 < p_{\mathrm{T}} < 3$	$-3.25 < y^* < -2.50$	$0.10 \pm 0.01 \pm 0.01$
$2 < p_{\mathrm{T}} < 3$	$-4.00 < y^* < -3.25$	$0.09 \pm 0.01 \pm 0.01$
$2 < p_{\mathrm{T}} < 3$	$-5.00 < y^* < -4.00$	$0.11 \pm 0.02 \pm 0.01$
$3 < p_{\mathrm{T}} < 4$	$-3.25 < y^* < -2.50$	$0.13 \pm 0.02 \pm 0.01$
$3 < p_{\mathrm{T}} < 4$	$-4.00 < y^* < -3.25$	$0.15 \pm 0.02 \pm 0.02$
$3 < p_{\mathrm{T}} < 4$	$-5.00 < y^* < -4.00$	$0.10 \pm 0.02 \pm 0.01$
$4 < p_{\mathrm{T}} < 5$	$-3.25 < y^* < -2.50$	$0.12 \pm 0.02 \pm 0.01$
$4 < p_{\mathrm{T}} < 5$	$-4.00 < y^* < -3.25$	$0.12 \pm 0.02 \pm 0.01$
$4 < p_{\mathrm{T}} < 5$	$-5.00 < y^* < -4.00$	$0.13 \pm 0.02 \pm 0.01$
$5 < p_{\mathrm{T}} < 6$	$-3.25 < y^* < -2.50$	$0.15 \pm 0.02 \pm 0.02$
$5 < p_{\mathrm{T}} < 6$	$-4.00 < y^* < -3.25$	$0.15 \pm 0.02 \pm 0.02$
$5 < p_{\mathrm{T}} < 6$	$-5.00 < y^* < -4.00$	$0.18 \pm 0.03 \pm 0.02$
$6 < p_{\mathrm{T}} < 7$	$-3.25 < y^* < -2.50$	$0.18 \pm 0.02 \pm 0.02$
$6 < p_{\mathrm{T}} < 7$	$-4.00 < y^* < -3.25$	$0.17 \pm 0.02 \pm 0.02$
$6 < p_{\mathrm{T}} < 7$	$-5.00 < y^* < -4.00$	$0.21 \pm 0.04 \pm 0.02$
$7 < p_{\mathrm{T}} < 8$	$-3.25 < y^* < -2.50$	$0.15 \pm 0.03 \pm 0.02$
$7 < p_{\mathrm{T}} < 8$	$-4.00 < y^* < -3.25$	$0.16 \pm 0.03 \pm 0.02$
$7 < p_{\mathrm{T}} < 8$	$-5.00 < y^* < -4.00$	$0.28 \pm 0.05 \pm 0.03$
$8 < p_{\mathrm{T}} < 10$	$-3.25 < y^* < -2.50$	$0.21 \pm 0.03 \pm 0.02$
$8 < p_{\mathrm{T}} < 10$	$-4.00 < y^* < -3.25$	$0.35 \pm 0.03 \pm 0.04$
$8 < p_{\mathrm{T}} < 10$	$-5.00 < y^* < -4.00$	$0.33 \pm 0.06 \pm 0.04$
$10 < p_{\mathrm{T}} < 14$	$-3.25 < y^* < -2.50$	$0.20 \pm 0.04 \pm 0.02$
$10 < p_{\mathrm{T}} < 14$	$-4.00 < y^* < -3.25$	$0.38 \pm 0.05 \pm 0.04$
$10 < p_{\mathrm{T}} < 14$	$-5.00 < y^* < -4.00$	$0.41 \pm 0.09 \pm 0.05$

Table 3. Cross-section ratios of $\psi(2S)$ over J/ψ prompt production in Pbp collisions. The first uncertainty is statistical and the second systematic.

JHEP04(2024)111

p_{T} interval (GeV/c)	y^* interval	$\sigma_{\psi(2S)}/\sigma_{J/\psi}$
$0 < p_{\mathrm{T}} < 1$	$1.50 < y^* < 2.50$	$0.19 \pm 0.06 \pm 0.02$
$0 < p_{\mathrm{T}} < 1$	$2.50 < y^* < 3.25$	$0.27 \pm 0.07 \pm 0.03$
$0 < p_{\mathrm{T}} < 1$	$3.25 < y^* < 4.00$	$0.07 \pm 0.05 \pm 0.01$
$1 < p_{\mathrm{T}} < 2$	$1.50 < y^* < 2.50$	$0.19 \pm 0.04 \pm 0.02$
$1 < p_{\mathrm{T}} < 2$	$2.50 < y^* < 3.25$	$0.28 \pm 0.05 \pm 0.03$
$1 < p_{\mathrm{T}} < 2$	$3.25 < y^* < 4.00$	$0.18 \pm 0.05 \pm 0.02$
$2 < p_{\mathrm{T}} < 3$	$1.50 < y^* < 2.50$	$0.18 \pm 0.03 \pm 0.02$
$2 < p_{\mathrm{T}} < 3$	$2.50 < y^* < 3.25$	$0.18 \pm 0.03 \pm 0.02$
$2 < p_{\mathrm{T}} < 3$	$3.25 < y^* < 4.00$	$0.29 \pm 0.05 \pm 0.03$
$3 < p_{\mathrm{T}} < 4$	$1.50 < y^* < 2.50$	$0.24 \pm 0.03 \pm 0.02$
$3 < p_{\mathrm{T}} < 4$	$2.50 < y^* < 3.25$	$0.25 \pm 0.03 \pm 0.02$
$3 < p_{\mathrm{T}} < 4$	$3.25 < y^* < 4.00$	$0.33 \pm 0.06 \pm 0.03$
$4 < p_{\mathrm{T}} < 5$	$1.50 < y^* < 2.50$	$0.27 \pm 0.04 \pm 0.03$
$4 < p_{\mathrm{T}} < 5$	$2.50 < y^* < 3.25$	$0.27 \pm 0.04 \pm 0.02$
$4 < p_{\mathrm{T}} < 5$	$3.25 < y^* < 4.00$	$0.33 \pm 0.07 \pm 0.03$
$5 < p_{\mathrm{T}} < 6$	$1.50 < y^* < 2.50$	$0.29 \pm 0.05 \pm 0.03$
$5 < p_{\mathrm{T}} < 6$	$2.50 < y^* < 3.25$	$0.43 \pm 0.05 \pm 0.04$
$5 < p_{\mathrm{T}} < 6$	$3.25 < y^* < 4.00$	$0.26 \pm 0.07 \pm 0.02$
$6 < p_{\mathrm{T}} < 7$	$1.50 < y^* < 2.50$	$0.35 \pm 0.06 \pm 0.03$
$6 < p_{\mathrm{T}} < 7$	$2.50 < y^* < 3.25$	$0.34 \pm 0.06 \pm 0.03$
$6 < p_{\mathrm{T}} < 7$	$3.25 < y^* < 4.00$	$0.36 \pm 0.09 \pm 0.03$
$7 < p_{\mathrm{T}} < 8$	$1.50 < y^* < 2.50$	$0.24 \pm 0.05 \pm 0.02$
$7 < p_{\mathrm{T}} < 8$	$2.50 < y^* < 3.25$	$0.27 \pm 0.06 \pm 0.02$
$7 < p_{\mathrm{T}} < 8$	$3.25 < y^* < 4.00$	$0.30 \pm 0.12 \pm 0.03$
$8 < p_{\mathrm{T}} < 10$	$1.50 < y^* < 2.50$	$0.28 \pm 0.05 \pm 0.03$
$8 < p_{\mathrm{T}} < 10$	$2.50 < y^* < 3.25$	$0.50 \pm 0.07 \pm 0.05$
$8 < p_{\mathrm{T}} < 10$	$3.25 < y^* < 4.00$	$0.49 \pm 0.12 \pm 0.05$
$10 < p_{\mathrm{T}} < 14$	$1.50 < y^* < 2.50$	$0.41 \pm 0.07 \pm 0.04$
$10 < p_{\mathrm{T}} < 14$	$2.50 < y^* < 3.25$	$0.43 \pm 0.08 \pm 0.04$
$10 < p_{\mathrm{T}} < 14$	$3.25 < y^* < 4.00$	$0.51 \pm 0.15 \pm 0.05$

Table 4. Cross-section ratios of $\psi(2S)$ over J/ψ nonprompt production in pPb collisions. The first uncertainty is statistical and the second systematic.

JHEP04(2024)111

p_{T} interval (GeV/c)	y^* interval	$\sigma_{\psi(2S)}/\sigma_{J/\psi}$
$0 < p_{\mathrm{T}} < 1$	$-3.25 < y^* < -2.50$	$0.22 \pm 0.08 \pm 0.03$
$0 < p_{\mathrm{T}} < 1$	$-4.00 < y^* < -3.25$	$0.23 \pm 0.06 \pm 0.03$
$0 < p_{\mathrm{T}} < 1$	$-5.00 < y^* < -4.00$	$0.11 \pm 0.07 \pm 0.01$
$1 < p_{\mathrm{T}} < 2$	$-3.25 < y^* < -2.50$	$0.32 \pm 0.05 \pm 0.04$
$1 < p_{\mathrm{T}} < 2$	$-4.00 < y^* < -3.25$	$0.20 \pm 0.03 \pm 0.02$
$1 < p_{\mathrm{T}} < 2$	$-5.00 < y^* < -4.00$	$0.11 \pm 0.03 \pm 0.01$
$2 < p_{\mathrm{T}} < 3$	$-3.25 < y^* < -2.50$	$0.23 \pm 0.04 \pm 0.03$
$2 < p_{\mathrm{T}} < 3$	$-4.00 < y^* < -3.25$	$0.24 \pm 0.04 \pm 0.03$
$2 < p_{\mathrm{T}} < 3$	$-5.00 < y^* < -4.00$	$0.20 \pm 0.05 \pm 0.02$
$3 < p_{\mathrm{T}} < 4$	$-3.25 < y^* < -2.50$	$0.36 \pm 0.05 \pm 0.04$
$3 < p_{\mathrm{T}} < 4$	$-4.00 < y^* < -3.25$	$0.23 \pm 0.04 \pm 0.02$
$3 < p_{\mathrm{T}} < 4$	$-5.00 < y^* < -4.00$	$0.36 \pm 0.07 \pm 0.04$
$4 < p_{\mathrm{T}} < 5$	$-3.25 < y^* < -2.50$	$0.39 \pm 0.05 \pm 0.04$
$4 < p_{\mathrm{T}} < 5$	$-4.00 < y^* < -3.25$	$0.24 \pm 0.04 \pm 0.02$
$4 < p_{\mathrm{T}} < 5$	$-5.00 < y^* < -4.00$	$0.32 \pm 0.07 \pm 0.03$
$5 < p_{\mathrm{T}} < 6$	$-3.25 < y^* < -2.50$	$0.32 \pm 0.06 \pm 0.03$
$5 < p_{\mathrm{T}} < 6$	$-4.00 < y^* < -3.25$	$0.30 \pm 0.05 \pm 0.03$
$5 < p_{\mathrm{T}} < 6$	$-5.00 < y^* < -4.00$	$0.27 \pm 0.08 \pm 0.03$
$6 < p_{\mathrm{T}} < 7$	$-3.25 < y^* < -2.50$	$0.32 \pm 0.06 \pm 0.03$
$6 < p_{\mathrm{T}} < 7$	$-4.00 < y^* < -3.25$	$0.31 \pm 0.06 \pm 0.03$
$6 < p_{\mathrm{T}} < 7$	$-5.00 < y^* < -4.00$	$0.29 \pm 0.10 \pm 0.03$
$7 < p_{\mathrm{T}} < 8$	$-3.25 < y^* < -2.50$	$0.26 \pm 0.07 \pm 0.03$
$7 < p_{\mathrm{T}} < 8$	$-4.00 < y^* < -3.25$	$0.41 \pm 0.08 \pm 0.04$
$7 < p_{\mathrm{T}} < 8$	$-5.00 < y^* < -4.00$	$0.20 \pm 0.12 \pm 0.02$
$8 < p_{\mathrm{T}} < 10$	$-3.25 < y^* < -2.50$	$0.33 \pm 0.06 \pm 0.03$
$8 < p_{\mathrm{T}} < 10$	$-4.00 < y^* < -3.25$	$0.27 \pm 0.07 \pm 0.03$
$8 < p_{\mathrm{T}} < 10$	$-5.00 < y^* < -4.00$	$0.21 \pm 0.13 \pm 0.03$
$10 < p_{\mathrm{T}} < 14$	$-3.25 < y^* < -2.50$	$0.21 \pm 0.06 \pm 0.02$
$10 < p_{\mathrm{T}} < 14$	$-4.00 < y^* < -3.25$	$0.34 \pm 0.09 \pm 0.04$
$10 < p_{\mathrm{T}} < 14$	$-5.00 < y^* < -4.00$	$0.45 \pm 0.21 \pm 0.06$

Table 5. Cross-section ratios of $\psi(2S)$ over J/ψ nonprompt production in Pbp collisions. The first uncertainty is statistical and the second systematic.

JHEP04(2024)111

p_{T} interval (GeV/c)	$\sigma_{\psi(2S)}/\sigma_{J/\psi}$
$0 < p_{\mathrm{T}} < 1$	$0.08 \pm 0.01 \pm 0.01$
$1 < p_{\mathrm{T}} < 2$	$0.09 \pm 0.01 \pm 0.01$
$2 < p_{\mathrm{T}} < 3$	$0.12 \pm 0.01 \pm 0.01$
$3 < p_{\mathrm{T}} < 4$	$0.14 \pm 0.01 \pm 0.01$
$4 < p_{\mathrm{T}} < 5$	$0.16 \pm 0.01 \pm 0.01$
$5 < p_{\mathrm{T}} < 6$	$0.18 \pm 0.01 \pm 0.02$
$6 < p_{\mathrm{T}} < 7$	$0.19 \pm 0.02 \pm 0.02$
$7 < p_{\mathrm{T}} < 8$	$0.26 \pm 0.02 \pm 0.02$
$8 < p_{\mathrm{T}} < 10$	$0.27 \pm 0.02 \pm 0.02$
$10 < p_{\mathrm{T}} < 14$	$0.23 \pm 0.03 \pm 0.02$

Table 6. Cross-section ratios of $\psi(2S)$ over J/ψ prompt production in pPb collisions, as a function of p_{T}, integrated over y^*. The first uncertainty is statistical and the second systematic.

p_{T} interval (GeV/c)	$\sigma_{\psi(2S)}/\sigma_{J/\psi}$
$0 < p_{\mathrm{T}} < 1$	$0.07 \pm 0.01 \pm 0.01$
$1 < p_{\mathrm{T}} < 2$	$0.11 \pm 0.01 \pm 0.01$
$2 < p_{\mathrm{T}} < 3$	$0.11 \pm 0.01 \pm 0.01$
$3 < p_{\mathrm{T}} < 4$	$0.15 \pm 0.01 \pm 0.01$
$4 < p_{\mathrm{T}} < 5$	$0.14 \pm 0.01 \pm 0.01$
$5 < p_{\mathrm{T}} < 6$	$0.17 \pm 0.01 \pm 0.02$
$6 < p_{\mathrm{T}} < 7$	$0.21 \pm 0.02 \pm 0.02$
$7 < p_{\mathrm{T}} < 8$	$0.20 \pm 0.02 \pm 0.02$
$8 < p_{\mathrm{T}} < 10$	$0.32 \pm 0.02 \pm 0.03$
$10 < p_{\mathrm{T}} < 14$	$0.32 \pm 0.04 \pm 0.03$

Table 7. Cross-section ratios of $\psi(2S)$ over J/ψ prompt production in Pbp collisions, as a function of p_{T}, integrated over y^*. The first uncertainty is statistical and the second systematic.

JHEP04(2024)111

p_{T} interval (GeV/c)	$\sigma_{\psi(2S)}/\sigma_{J/\psi}$
$0 < p_{\mathrm{T}} < 1$	$0.18 \pm 0.04 \pm 0.02$
$1 < p_{\mathrm{T}} < 2$	$0.21 \pm 0.02 \pm 0.02$
$2 < p_{\mathrm{T}} < 3$	$0.20 \pm 0.02 \pm 0.02$
$3 < p_{\mathrm{T}} < 4$	$0.27 \pm 0.02 \pm 0.03$
$4 < p_{\mathrm{T}} < 5$	$0.29 \pm 0.03 \pm 0.03$
$5 < p_{\mathrm{T}} < 6$	$0.33 \pm 0.03 \pm 0.03$
$6 < p_{\mathrm{T}} < 7$	$0.35 \pm 0.04 \pm 0.03$
$7 < p_{\mathrm{T}} < 8$	$0.24 \pm 0.04 \pm 0.02$
$8 < p_{\mathrm{T}} < 10$	$0.37 \pm 0.04 \pm 0.03$
$10 < p_{\mathrm{T}} < 14$	$0.43 \pm 0.05 \pm 0.04$

Table 8. Cross-section ratios of $\psi(2S)$ over J/ψ nonprompt production in pPb collisions, as a function of p_{T}, integrated over y^*. The first uncertainty is statistical and the second systematic.

p_{T} interval (GeV/c)	$\sigma_{\psi(2S)}/\sigma_{J/\psi}$
$0 < p_{\mathrm{T}} < 1$	$0.20 \pm 0.04 \pm 0.02$
$1 < p_{\mathrm{T}} < 2$	$0.23 \pm 0.03 \pm 0.03$
$2 < p_{\mathrm{T}} < 3$	$0.24 \pm 0.03 \pm 0.03$
$3 < p_{\mathrm{T}} < 4$	$0.35 \pm 0.03 \pm 0.03$
$4 < p_{\mathrm{T}} < 5$	$0.34 \pm 0.03 \pm 0.03$
$5 < p_{\mathrm{T}} < 6$	$0.32 \pm 0.04 \pm 0.03$
$6 < p_{\mathrm{T}} < 7$	$0.32 \pm 0.04 \pm 0.03$
$7 < p_{\mathrm{T}} < 8$	$0.31 \pm 0.05 \pm 0.03$
$8 < p_{\mathrm{T}} < 10$	$0.32 \pm 0.05 \pm 0.03$
$10 < p_{\mathrm{T}} < 14$	$0.29 \pm 0.05 \pm 0.03$

Table 9. Cross-section ratios of $\psi(2S)$ over J/ψ nonprompt production in Pbp collisions, as a function of p_{T}, integrated over y^*. The first uncertainty is statistical and the second systematic.

JHEP04(2024)111

y^* interval	$\sigma_{\psi(2S)}/\sigma_{J/\psi}$
$-3.25 < y^* < -2.50$	$0.11 \pm 0.01 \pm 0.01$
$-4.00 < y^* < -3.25$	$0.10 \pm 0.01 \pm 0.01$
$-5.00 < y^* < -4.00$	$0.12 \pm 0.01 \pm 0.01$
$1.50 < y^* < 2.50$	$0.12 \pm 0.01 \pm 0.01$
$2.50 < y^* < 3.25$	$0.12 \pm 0.01 \pm 0.01$
$3.25 < y^* < 4.00$	$0.13 \pm 0.01 \pm 0.01$

Table 10. Cross-section ratios of $\psi(2S)$ over J/ψ prompt production, as a function of y^*, integrated over p_{T}. The first uncertainty is statistical and the second systematic.

y^* interval	$\sigma_{\psi(2S)}/\sigma_{J/\psi}$
$-3.25 < y^* < -2.50$	$0.32 \pm 0.02 \pm 0.03$
$-4.00 < y^* < -3.25$	$0.24 \pm 0.02 \pm 0.03$
$-5.00 < y^* < -4.00$	$0.22 \pm 0.02 \pm 0.02$
$1.50 < y^* < 2.50$	$0.23 \pm 0.01 \pm 0.02$
$2.50 < y^* < 3.25$	$0.27 \pm 0.02 \pm 0.03$
$3.25 < y^* < 4.00$	$0.26 \pm 0.02 \pm 0.02$

Table 11. Cross-section ratios of $\psi(2S)$ over J/ψ nonprompt production, as a function of y^*, integrated over p_{T}. The first uncertainty is statistical and the second systematic.

JHEP04(2024)111

B Absolute $\psi(2S)$ cross-sections

p_{T} interval (GeV/c)	y^* interval	$\mathrm{d}^2\sigma/(\mathrm{d}y^*\mathrm{d}p_{\mathrm{T}})$ [nb/(GeV/c)]
$0 < p_{\mathrm{T}} < 1$	$1.50 < y^* < 2.50$	$7583 \pm 2196 \pm 1094$
$0 < p_{\mathrm{T}} < 1$	$2.50 < y^* < 3.25$	$6311 \pm 1628 \pm 674$
$0 < p_{\mathrm{T}} < 1$	$3.25 < y^* < 4.00$	$7599 \pm 1529 \pm 934$
$1 < p_{\mathrm{T}} < 2$	$1.50 < y^* < 2.50$	$20666 \pm 3108 \pm 2673$
$1 < p_{\mathrm{T}} < 2$	$2.50 < y^* < 3.25$	$12453 \pm 2175 \pm 1351$
$1 < p_{\mathrm{T}} < 2$	$3.25 < y^* < 4.00$	$10852 \pm 2057 \pm 1222$
$2 < p_{\mathrm{T}} < 3$	$1.50 < y^* < 2.50$	$19380 \pm 2772 \pm 2430$
$2 < p_{\mathrm{T}} < 3$	$2.50 < y^* < 3.25$	$20220 \pm 2386 \pm 2178$
$2 < p_{\mathrm{T}} < 3$	$3.25 < y^* < 4.00$	$14116 \pm 1991 \pm 1584$
$3 < p_{\mathrm{T}} < 4$	$1.50 < y^* < 2.50$	$20058 \pm 2118 \pm 2294$
$3 < p_{\mathrm{T}} < 4$	$2.50 < y^* < 3.25$	$11529 \pm 1567 \pm 1200$
$3 < p_{\mathrm{T}} < 4$	$3.25 < y^* < 4.00$	$11643 \pm 1525 \pm 1232$
$4 < p_{\mathrm{T}} < 5$	$1.50 < y^* < 2.50$	$11912 \pm 1455 \pm 1292$
$4 < p_{\mathrm{T}} < 5$	$2.50 < y^* < 3.25$	$10620 \pm 1043 \pm 1069$
$4 < p_{\mathrm{T}} < 5$	$3.25 < y^* < 4.00$	$6561 \pm 945 \pm 665$
$5 < p_{\mathrm{T}} < 6$	$1.50 < y^* < 2.50$	$6438 \pm 814 \pm 682$
$5 < p_{\mathrm{T}} < 6$	$2.50 < y^* < 3.25$	$6758 \pm 683 \pm 677$
$5 < p_{\mathrm{T}} < 6$	$3.25 < y^* < 4.00$	$4930 \pm 687 \pm 493$
$6 < p_{\mathrm{T}} < 7$	$1.50 < y^* < 2.50$	$4281 \pm 553 \pm 453$
$6 < p_{\mathrm{T}} < 7$	$2.50 < y^* < 3.25$	$3205 \pm 407 \pm 323$
$6 < p_{\mathrm{T}} < 7$	$3.25 < y^* < 4.00$	$2972 \pm 437 \pm 310$
$7 < p_{\mathrm{T}} < 8$	$1.50 < y^* < 2.50$	$3330 \pm 412 \pm 348$
$7 < p_{\mathrm{T}} < 8$	$2.50 < y^* < 3.25$	$2399 \pm 310 \pm 245$
$7 < p_{\mathrm{T}} < 8$	$3.25 < y^* < 4.00$	$2217 \pm 357 \pm 241$
$8 < p_{\mathrm{T}} < 10$	$1.50 < y^* < 2.50$	$1758 \pm 187 \pm 184$
$8 < p_{\mathrm{T}} < 10$	$2.50 < y^* < 3.25$	$1199 \pm 145 \pm 122$
$8 < p_{\mathrm{T}} < 10$	$3.25 < y^* < 4.00$	$605 \pm 124 \pm 70$
$10 < p_{\mathrm{T}} < 14$	$1.50 < y^* < 2.50$	$351 \pm 55 \pm 36$
$10 < p_{\mathrm{T}} < 14$	$2.50 < y^* < 3.25$	$194 \pm 47 \pm 20$
$10 < p_{\mathrm{T}} < 14$	$3.25 < y^* < 4.00$	$229 \pm 55 \pm 28$

Table 12. Absolute $\psi(2S)$ prompt production cross-section in pPb collisions. The first uncertainty is statistical and the second systematic.

JHEP04(2024)111

p_{T} interval (GeV/c)	y^* interval	$\mathrm{d}^2\sigma/(\mathrm{d}y^*\mathrm{d}p_{\mathrm{T}})$ [nb/(GeV/c)]
$0 < p_{\mathrm{T}} < 1$	$-3.25 < y^* < -2.50$	$8376 \pm 2712 \pm 1346$
$0 < p_{\mathrm{T}} < 1$	$-4.00 < y^* < -3.25$	$6593 \pm 1894 \pm 886$
$0 < p_{\mathrm{T}} < 1$	$-5.00 < y^* < -4.00$	$4716 \pm 1638 \pm 608$
$1 < p_{\mathrm{T}} < 2$	$-3.25 < y^* < -2.50$	$27207 \pm 3822 \pm 4113$
$1 < p_{\mathrm{T}} < 2$	$-4.00 < y^* < -3.25$	$12760 \pm 1979 \pm 1670$
$1 < p_{\mathrm{T}} < 2$	$-5.00 < y^* < -4.00$	$18484 \pm 2313 \pm 2285$
$2 < p_{\mathrm{T}} < 3$	$-3.25 < y^* < -2.50$	$23515 \pm 3270 \pm 3167$
$2 < p_{\mathrm{T}} < 3$	$-4.00 < y^* < -3.25$	$15894 \pm 2480 \pm 2017$
$2 < p_{\mathrm{T}} < 3$	$-5.00 < y^* < -4.00$	$12462 \pm 1988 \pm 1543$
$3 < p_{\mathrm{T}} < 4$	$-3.25 < y^* < -2.50$	$19105 \pm 2442 \pm 2376$
$3 < p_{\mathrm{T}} < 4$	$-4.00 < y^* < -3.25$	$16264 \pm 1872 \pm 1941$
$3 < p_{\mathrm{T}} < 4$	$-5.00 < y^* < -4.00$	$6856 \pm 1316 \pm 828$
$4 < p_{\mathrm{T}} < 5$	$-3.25 < y^* < -2.50$	$9423 \pm 1413 \pm 1092$
$4 < p_{\mathrm{T}} < 5$	$-4.00 < y^* < -3.25$	$7576 \pm 1030 \pm 897$
$4 < p_{\mathrm{T}} < 5$	$-5.00 < y^* < -4.00$	$4467 \pm 773 \pm 536$
$5 < p_{\mathrm{T}} < 6$	$-3.25 < y^* < -2.50$	$6512 \pm 847 \pm 755$
$5 < p_{\mathrm{T}} < 6$	$-4.00 < y^* < -3.25$	$4432 \pm 549 \pm 528$
$5 < p_{\mathrm{T}} < 6$	$-5.00 < y^* < -4.00$	$3061 \pm 450 \pm 368$
$6 < p_{\mathrm{T}} < 7$	$-3.25 < y^* < -2.50$	$4063 \pm 552 \pm 490$
$6 < p_{\mathrm{T}} < 7$	$-4.00 < y^* < -3.25$	$2875 \pm 347 \pm 335$
$6 < p_{\mathrm{T}} < 7$	$-5.00 < y^* < -4.00$	$1769 \pm 297 \pm 217$
$7 < p_{\mathrm{T}} < 8$	$-3.25 < y^* < -2.50$	$1837 \pm 327 \pm 222$
$7 < p_{\mathrm{T}} < 8$	$-4.00 < y^* < -3.25$	$1317 \pm 219 \pm 161$
$7 < p_{\mathrm{T}} < 8$	$-5.00 < y^* < -4.00$	$1080 \pm 179 \pm 145$
$8 < p_{\mathrm{T}} < 10$	$-3.25 < y^* < -2.50$	$1105 \pm 151 \pm 133$
$8 < p_{\mathrm{T}} < 10$	$-4.00 < y^* < -3.25$	$1200 \pm 115 \pm 144$
$8 < p_{\mathrm{T}} < 10$	$-5.00 < y^* < -4.00$	$449 \pm 74 \pm 65$
$10 < p_{\mathrm{T}} < 14$	$-3.25 < y^* < -2.50$	$240 \pm 47 \pm 31$
$10 < p_{\mathrm{T}} < 14$	$-4.00 < y^* < -3.25$	$262 \pm 36 \pm 34$
$10 < p_{\mathrm{T}} < 14$	$-5.00 < y^* < -4.00$	$95 \pm 21 \pm 14$

Table 13. Absolute $\psi(2S)$ prompt production cross-section in Pbp collisions. The first uncertainty is statistical and the second systematic.

JHEP04(2024)111

p_T interval (GeV/c)	y^* interval	$d^2\sigma/(dy^* dp_T)$ [nb/(GeV/c)]
$0 < p_T < 1$	$1.50 < y^* < 2.50$	$2692 \pm 798 \pm 389$
$0 < p_T < 1$	$2.50 < y^* < 3.25$	$2666 \pm 688 \pm 285$
$0 < p_T < 1$	$3.25 < y^* < 4.00$	$592 \pm 445 \pm 73$
$1 < p_T < 2$	$1.50 < y^* < 2.50$	$5911 \pm 1111 \pm 764$
$1 < p_T < 2$	$2.50 < y^* < 3.25$	$6634 \pm 1097 \pm 720$
$1 < p_T < 2$	$3.25 < y^* < 4.00$	$3446 \pm 891 \pm 388$
$2 < p_T < 3$	$1.50 < y^* < 2.50$	$5705 \pm 1084 \pm 715$
$2 < p_T < 3$	$2.50 < y^* < 3.25$	$4484 \pm 820 \pm 483$
$2 < p_T < 3$	$3.25 < y^* < 4.00$	$4965 \pm 878 \pm 557$
$3 < p_T < 4$	$1.50 < y^* < 2.50$	$6062 \pm 789 \pm 693$
$3 < p_T < 4$	$2.50 < y^* < 3.25$	$4521 \pm 613 \pm 471$
$3 < p_T < 4$	$3.25 < y^* < 4.00$	$4220 \pm 807 \pm 446$
$4 < p_T < 5$	$1.50 < y^* < 2.50$	$4419 \pm 630 \pm 479$
$4 < p_T < 5$	$2.50 < y^* < 3.25$	$3105 \pm 442 \pm 312$
$4 < p_T < 5$	$3.25 < y^* < 4.00$	$2535 \pm 563 \pm 257$
$5 < p_T < 6$	$1.50 < y^* < 2.50$	$2841 \pm 449 \pm 301$
$5 < p_T < 6$	$2.50 < y^* < 3.25$	$3092 \pm 384 \pm 310$
$5 < p_T < 6$	$3.25 < y^* < 4.00$	$1156 \pm 289 \pm 116$
$6 < p_T < 7$	$1.50 < y^* < 2.50$	$2107 \pm 336 \pm 223$
$6 < p_T < 7$	$2.50 < y^* < 3.25$	$1521 \pm 251 \pm 153$
$6 < p_T < 7$	$3.25 < y^* < 4.00$	$924 \pm 233 \pm 96$
$7 < p_T < 8$	$1.50 < y^* < 2.50$	$784 \pm 175 \pm 82$
$7 < p_T < 8$	$2.50 < y^* < 3.25$	$786 \pm 166 \pm 80$
$7 < p_T < 8$	$3.25 < y^* < 4.00$	$496 \pm 191 \pm 54$
$8 < p_T < 10$	$1.50 < y^* < 2.50$	$573 \pm 102 \pm 60$
$8 < p_T < 10$	$2.50 < y^* < 3.25$	$675 \pm 95 \pm 69$
$8 < p_T < 10$	$3.25 < y^* < 4.00$	$404 \pm 96 \pm 47$
$10 < p_T < 14$	$1.50 < y^* < 2.50$	$263 \pm 43 \pm 27$
$10 < p_T < 14$	$2.50 < y^* < 3.25$	$186 \pm 36 \pm 19$
$10 < p_T < 14$	$3.25 < y^* < 4.00$	$118 \pm 33 \pm 14$

Table 14. Absolute $\psi(2S)$ nonprompt production cross-section in pPb collisions. The first uncertainty is statistical and the second systematic.

JHEP04(2024)111

p_{T} interval (GeV/c)	y^* interval	$\mathrm{d}^2\sigma/(\mathrm{d}y^*\mathrm{d}p_{\mathrm{T}})$ [nb/(GeV/c)]
$0 < p_{\mathrm{T}} < 1$	$-3.25 < y^* < -2.50$	$3257 \pm 118 \pm 523$
$0 < p_{\mathrm{T}} < 1$	$-4.00 < y^* < -3.25$	$2564 \pm 625 \pm 345$
$0 < p_{\mathrm{T}} < 1$	$-5.00 < y^* < -4.00$	$753 \pm 469 \pm 97$
$1 < p_{\mathrm{T}} < 2$	$-3.25 < y^* < -2.50$	$10845 \pm 1677 \pm 1639$
$1 < p_{\mathrm{T}} < 2$	$-4.00 < y^* < -3.25$	$3441 \pm 589 \pm 450$
$1 < p_{\mathrm{T}} < 2$	$-5.00 < y^* < -4.00$	$1504 \pm 441 \pm 186$
$2 < p_{\mathrm{T}} < 3$	$-3.25 < y^* < -2.50$	$7165 \pm 1217 \pm 965$
$2 < p_{\mathrm{T}} < 3$	$-4.00 < y^* < -3.25$	$5337 \pm 873 \pm 677$
$2 < p_{\mathrm{T}} < 3$	$-5.00 < y^* < -4.00$	$2438 \pm 562 \pm 302$
$3 < p_{\mathrm{T}} < 4$	$-3.25 < y^* < -2.50$	$8195 \pm 1017 \pm 1019$
$3 < p_{\mathrm{T}} < 4$	$-4.00 < y^* < -3.25$	$3767 \pm 567 \pm 450$
$3 < p_{\mathrm{T}} < 4$	$-5.00 < y^* < -4.00$	$2765 \pm 522 \pm 334$
$4 < p_{\mathrm{T}} < 5$	$-3.25 < y^* < -2.50$	$5532 \pm 660 \pm 641$
$4 < p_{\mathrm{T}} < 5$	$-4.00 < y^* < -3.25$	$2142 \pm 382 \pm 254$
$4 < p_{\mathrm{T}} < 5$	$-5.00 < y^* < -4.00$	$1376 \pm 294 \pm 165$
$5 < p_{\mathrm{T}} < 6$	$-3.25 < y^* < -2.50$	$2565 \pm 446 \pm 297$
$5 < p_{\mathrm{T}} < 6$	$-4.00 < y^* < -3.25$	$1563 \pm 242 \pm 186$
$5 < p_{\mathrm{T}} < 6$	$-5.00 < y^* < -4.00$	$598 \pm 170 \pm 72$
$6 < p_{\mathrm{T}} < 7$	$-3.25 < y^* < -2.50$	$1482 \pm 291 \pm 179$
$6 < p_{\mathrm{T}} < 7$	$-4.00 < y^* < -3.25$	$926 \pm 166 \pm 108$
$6 < p_{\mathrm{T}} < 7$	$-5.00 < y^* < -4.00$	$352 \pm 120 \pm 43$
$7 < p_{\mathrm{T}} < 8$	$-3.25 < y^* < -2.50$	$707 \pm 182 \pm 85$
$7 < p_{\mathrm{T}} < 8$	$-4.00 < y^* < -3.25$	$718 \pm 139 \pm 88$
$7 < p_{\mathrm{T}} < 8$	$-5.00 < y^* < -4.00$	$117 \pm 67 \pm 16$
$8 < p_{\mathrm{T}} < 10$	$-3.25 < y^* < -2.50$	$519 \pm 99 \pm 63$
$8 < p_{\mathrm{T}} < 10$	$-4.00 < y^* < -3.25$	$215 \pm 55 \pm 26$
$8 < p_{\mathrm{T}} < 10$	$-5.00 < y^* < -4.00$	$56 \pm 33 \pm 8$
$10 < p_{\mathrm{T}} < 14$	$-3.25 < y^* < -2.50$	$98 \pm 27 \pm 13$
$10 < p_{\mathrm{T}} < 14$	$-4.00 < y^* < -3.25$	$76 \pm 20 \pm 10$
$10 < p_{\mathrm{T}} < 14$	$-5.00 < y^* < -4.00$	$27 \pm 12 \pm 4$

Table 15. Absolute $\psi(2S)$ nonprompt production cross-section in Pbp collisions. The first uncertainty is statistical and the second systematic.

JHEP04(2024)111

p_{T} interval (GeV/c)	$\mathrm{d}\sigma/\mathrm{d}p_{\mathrm{T}}$ [nb/(GeV/c)]
$0 < p_{\mathrm{T}} < 1$	$18015 \pm 2762 \pm 656$
$1 < p_{\mathrm{T}} < 2$	$38145 \pm 3834 \pm 1595$
$2 < p_{\mathrm{T}} < 3$	$45132 \pm 3621 \pm 1495$
$3 < p_{\mathrm{T}} < 4$	$37437 \pm 2679 \pm 1380$
$4 < p_{\mathrm{T}} < 5$	$24798 \pm 1797 \pm 905$
$5 < p_{\mathrm{T}} < 6$	$15204 \pm 1091 \pm 618$
$6 < p_{\mathrm{T}} < 7$	$8914 \pm 712 \pm 408$
$7 < p_{\mathrm{T}} < 8$	$6792 \pm 544 \pm 180$
$8 < p_{\mathrm{T}} < 10$	$3111 \pm 236 \pm 145$
$10 < p_{\mathrm{T}} < 14$	$669 \pm 78 \pm 51$

Table 16. Absolute $\psi(2S)$ prompt production cross-section in pPb collisions, as a function of p_{T}, integrated over y^*. The first uncertainty is statistical and the second systematic.

p_{T} interval (GeV/c)	$\mathrm{d}\sigma/\mathrm{d}p_{\mathrm{T}}$ [nb/(GeV/c)]
$0 < p_{\mathrm{T}} < 1$	$16857 \pm 3298 \pm 4383$
$1 < p_{\mathrm{T}} < 2$	$50640 \pm 4452 \pm 11141$
$2 < p_{\mathrm{T}} < 3$	$44782 \pm 4047 \pm 5822$
$3 < p_{\mathrm{T}} < 4$	$36445 \pm 2985 \pm 6560$
$4 < p_{\mathrm{T}} < 5$	$18454 \pm 1711 \pm 4245$
$5 < p_{\mathrm{T}} < 6$	$12132 \pm 1001 \pm 2548$
$6 < p_{\mathrm{T}} < 7$	$7547 \pm 649 \pm 1660$
$7 < p_{\mathrm{T}} < 8$	$3635 \pm 390 \pm 836$
$8 < p_{\mathrm{T}} < 10$	$2343 \pm 183 \pm 422$
$10 < p_{\mathrm{T}} < 14$	$507 \pm 57 \pm 76$

Table 17. Absolute $\psi(2S)$ prompt production cross-section in Pbp collisions, as a function of p_{T}, integrated over y^*. The first uncertainty is statistical and the second systematic.

JHEP04(2024)111

p_{T} interval (GeV/c)	dσ/dp_{T} [nb/(GeV/c)]
$0 < p_{\mathrm{T}} < 1$	$5136 \pm 1007 \pm 656$
$1 < p_{\mathrm{T}} < 2$	$13471 \pm 1535 \pm 1595$
$2 < p_{\mathrm{T}} < 3$	$12791 \pm 1409 \pm 1495$
$3 < p_{\mathrm{T}} < 4$	$12617 \pm 1096 \pm 1380$
$4 < p_{\mathrm{T}} < 5$	$8648 \pm 828 \pm 905$
$5 < p_{\mathrm{T}} < 6$	$6027 \pm 575 \pm 618$
$6 < p_{\mathrm{T}} < 7$	$3940 \pm 423 \pm 408$
$7 < p_{\mathrm{T}} < 8$	$1745 \pm 258 \pm 180$
$8 < p_{\mathrm{T}} < 10$	$1383 \pm 144 \pm 145$
$10 < p_{\mathrm{T}} < 14$	$491 \pm 57 \pm 51$

Table 18. Absolute $\psi(2S)$ nonprompt production cross-section in pPb collisions, as a function of p_{T}, integrated over y^*. The first uncertainty is statistical and the second systematic.

p_{T} interval (GeV/c)	dσ/dp_{T} [nb/(GeV/c)]
$0 < p_{\mathrm{T}} < 1$	$5119 \pm 1109 \pm 1329$
$1 < p_{\mathrm{T}} < 2$	$12219 \pm 1404 \pm 2706$
$2 < p_{\mathrm{T}} < 3$	$11814 \pm 1256 \pm 1574$
$3 < p_{\mathrm{T}} < 4$	$11737 \pm 1017 \pm 2145$
$4 < p_{\mathrm{T}} < 5$	$7132 \pm 643 \pm 1645$
$5 < p_{\mathrm{T}} < 6$	$3694 \pm 417 \pm 804$
$6 < p_{\mathrm{T}} < 7$	$2157 \pm 279 \pm 493$
$7 < p_{\mathrm{T}} < 8$	$1186 \pm 184 \pm 275$
$8 < p_{\mathrm{T}} < 10$	$606 \pm 91 \pm 114$
$10 < p_{\mathrm{T}} < 14$	$158 \pm 28 \pm 24$

Table 19. Absolute $\psi(2S)$ nonprompt production cross-section in Pbp collisions, as a function of p_{T}, integrated over y^*. The first uncertainty is statistical and the second systematic.

JHEP04(2024)111

C $\psi(2S)$ nuclear modification factors

p_{T} interval (GeV/c)	$R_{p\mathrm{Pb}}$
$0 < p_{\mathrm{T}} < 1$	$0.42 \pm 0.07 \pm 0.07$
$1 < p_{\mathrm{T}} < 2$	$0.39 \pm 0.04 \pm 0.07$
$2 < p_{\mathrm{T}} < 3$	$0.52 \pm 0.04 \pm 0.08$
$3 < p_{\mathrm{T}} < 4$	$0.59 \pm 0.04 \pm 0.09$
$4 < p_{\mathrm{T}} < 5$	$0.63 \pm 0.05 \pm 0.10$
$5 < p_{\mathrm{T}} < 6$	$0.66 \pm 0.05 \pm 0.10$
$6 < p_{\mathrm{T}} < 7$	$0.62 \pm 0.05 \pm 0.11$
$7 < p_{\mathrm{T}} < 8$	$0.88 \pm 0.07 \pm 0.12$
$8 < p_{\mathrm{T}} < 10$	$0.85 \pm 0.08 \pm 0.12$
$10 < p_{\mathrm{T}} < 14$	$0.58 \pm 0.08 \pm 0.13$

Table 20. Prompt $\psi(2S)$ modification factor $R_{p\mathrm{Pb}}$ in pPb collisions, as a function of p_{T}, integrated over y^*. The first uncertainty is statistical and the second systematic.

p_{T} interval (GeV/c)	$R_{p\mathrm{Pb}}$
$0 < p_{\mathrm{T}} < 1$	$0.48 \pm 0.09 \pm 0.12$
$1 < p_{\mathrm{T}} < 2$	$0.66 \pm 0.06 \pm 0.12$
$2 < p_{\mathrm{T}} < 3$	$0.71 \pm 0.06 \pm 0.14$
$3 < p_{\mathrm{T}} < 4$	$0.82 \pm 0.07 \pm 0.16$
$4 < p_{\mathrm{T}} < 5$	$0.71 \pm 0.07 \pm 0.17$
$5 < p_{\mathrm{T}} < 6$	$0.84 \pm 0.07 \pm 0.18$
$6 < p_{\mathrm{T}} < 7$	$0.87 \pm 0.08 \pm 0.19$
$7 < p_{\mathrm{T}} < 8$	$0.81 \pm 0.09 \pm 0.20$
$8 < p_{\mathrm{T}} < 10$	$1.19 \pm 0.12 \pm 0.21$
$10 < p_{\mathrm{T}} < 14$	$0.88 \pm 0.11 \pm 0.22$

Table 21. Prompt $\psi(2S)$ modification factor $R_{p\mathrm{Pb}}$ in Pbp collisions, as a function of p_{T}, integrated over y^*. The first uncertainty is statistical and the second systematic.

JHEP04(2024)111

p_{T} interval (GeV/c)	$R_{p\mathrm{Pb}}$
$0 < p_{\mathrm{T}} < 1$	$0.88 \pm 0.19 \pm 0.13$
$1 < p_{\mathrm{T}} < 2$	$0.72 \pm 0.08 \pm 0.10$
$2 < p_{\mathrm{T}} < 3$	$0.78 \pm 0.09 \pm 0.11$
$3 < p_{\mathrm{T}} < 4$	$0.98 \pm 0.09 \pm 0.12$
$4 < p_{\mathrm{T}} < 5$	$0.86 \pm 0.09 \pm 0.12$
$5 < p_{\mathrm{T}} < 6$	$1.00 \pm 0.10 \pm 0.13$
$6 < p_{\mathrm{T}} < 7$	$1.15 \pm 0.13 \pm 0.14$
$7 < p_{\mathrm{T}} < 8$	$0.82 \pm 0.14 \pm 0.15$
$8 < p_{\mathrm{T}} < 10$	$1.20 \pm 0.15 \pm 0.15$
$10 < p_{\mathrm{T}} < 14$	$1.18 \pm 0.16 \pm 0.16$

Table 22. Nonprompt $\psi(2S)$ modification factor $R_{p\mathrm{Pb}}$ in pPb collisions, as a function of p_{T}, integrated over y^*. The first uncertainty is statistical and the second systematic.

p_{T} interval (GeV/c)	$R_{p\mathrm{Pb}}$
$0 < p_{\mathrm{T}} < 1$	$1.41 \pm 0.33 \pm 0.21$
$1 < p_{\mathrm{T}} < 2$	$1.04 \pm 0.12 \pm 0.18$
$2 < p_{\mathrm{T}} < 3$	$1.19 \pm 0.13 \pm 0.18$
$3 < p_{\mathrm{T}} < 4$	$1.62 \pm 0.15 \pm 0.20$
$4 < p_{\mathrm{T}} < 5$	$1.31 \pm 0.12 \pm 0.21$
$5 < p_{\mathrm{T}} < 6$	$1.13 \pm 0.13 \pm 0.21$
$6 < p_{\mathrm{T}} < 7$	$1.18 \pm 0.16 \pm 0.21$
$7 < p_{\mathrm{T}} < 8$	$1.06 \pm 0.18 \pm 0.21$
$8 < p_{\mathrm{T}} < 10$	$1.10 \pm 0.18 \pm 0.23$
$10 < p_{\mathrm{T}} < 14$	$0.86 \pm 0.17 \pm 0.26$

Table 23. Nonprompt $\psi(2S)$ modification factor $R_{p\mathrm{Pb}}$ in Pbp collisions, as a function of p_{T}, integrated over y^*. The first uncertainty is statistical and the second systematic.

JHEP04(2024)111

D $\psi(2S)$ forward-to-backward ratios

p_{T} interval (GeV/c)	R_{FB}
$0 < p_{\mathrm{T}} < 1$	$0.66 \pm 0.18 \pm 0.04$
$1 < p_{\mathrm{T}} < 2$	$0.37 \pm 0.06 \pm 0.02$
$2 < p_{\mathrm{T}} < 3$	$0.61 \pm 0.08 \pm 0.03$
$3 < p_{\mathrm{T}} < 4$	$0.45 \pm 0.06 \pm 0.02$
$4 < p_{\mathrm{T}} < 5$	$0.69 \pm 0.09 \pm 0.04$
$5 < p_{\mathrm{T}} < 6$	$0.70 \pm 0.09 \pm 0.04$
$6 < p_{\mathrm{T}} < 7$	$0.60 \pm 0.08 \pm 0.03$
$7 < p_{\mathrm{T}} < 8$	$0.93 \pm 0.15 \pm 0.05$
$8 < p_{\mathrm{T}} < 10$	$0.52 \pm 0.07 \pm 0.03$
$10 < p_{\mathrm{T}} < 14$	$0.55 \pm 0.12 \pm 0.03$

Table 24. Prompt $\psi(2S)$ forward to backward ratio R_{FB}, as a function of p_{T}, integrated over y^*. The first uncertainty is statistical and the second systematic.

p_{T} interval (GeV/c)	R_{FB}
$0 < p_{\mathrm{T}} < 1$	$0.41 \pm 0.14 \pm 0.02$
$1 < p_{\mathrm{T}} < 2$	$0.48 \pm 0.09 \pm 0.03$
$2 < p_{\mathrm{T}} < 3$	$0.53 \pm 0.09 \pm 0.03$
$3 < p_{\mathrm{T}} < 4$	$0.51 \pm 0.08 \pm 0.03$
$4 < p_{\mathrm{T}} < 5$	$0.49 \pm 0.08 \pm 0.03$
$5 < p_{\mathrm{T}} < 6$	$0.72 \pm 0.12 \pm 0.04$
$6 < p_{\mathrm{T}} < 7$	$0.67 \pm 0.13 \pm 0.04$
$7 < p_{\mathrm{T}} < 8$	$0.61 \pm 0.14 \pm 0.03$
$8 < p_{\mathrm{T}} < 10$	$0.99 \pm 0.20 \pm 0.06$
$10 < p_{\mathrm{T}} < 14$	$1.14 \pm 0.29 \pm 0.07$

Table 25. Nonprompt $\psi(2S)$ forward to backward ratio R_{FB}, as a function of p_{T}, integrated over y^*. The first uncertainty is statistical and the second systematic.

y^* interval	R_{FB}
$2.50 < y^* < 3.25$	$0.51 \pm 0.04 \pm 0.03$
$3.25 < y^* < 4.00$	$0.57 \pm 0.05 \pm 0.03$

Table 26. Prompt $\psi(2S)$ forward to backward ratio R_{FB}, as a function of y^*, integrated over p_{T}. The first uncertainty is statistical and the second systematic.

JHEP04(2024)111

y^* interval	R_{FB}
$2.50 < y^* < 3.25$	$0.50 \pm 0.05 \pm 0.03$
$3.25 < y^* < 4.00$	$0.61 \pm 0.07 \pm 0.03$

Table 27. Nonprompt $\psi(2S)$ forward to backward ratio R_{FB}, as a function of y^*, integrated over p_{T}. The first uncertainty is statistical and the second systematic.

E $\psi(2S)$ to J/ψ double cross-section ratios

p_{T} interval (GeV/c)	$R^{p\mathrm{Pb}}_{\psi(2S)/J/\psi}$
$0 < p_{\mathrm{T}} < 1$	$0.80 \pm 0.12 \pm 0.16$
$1 < p_{\mathrm{T}} < 2$	$0.70 \pm 0.07 \pm 0.12$
$2 < p_{\mathrm{T}} < 3$	$0.80 \pm 0.06 \pm 0.10$
$3 < p_{\mathrm{T}} < 4$	$0.82 \pm 0.06 \pm 0.09$
$4 < p_{\mathrm{T}} < 5$	$0.83 \pm 0.06 \pm 0.09$
$5 < p_{\mathrm{T}} < 6$	$0.81 \pm 0.06 \pm 0.09$
$6 < p_{\mathrm{T}} < 7$	$0.72 \pm 0.06 \pm 0.08$
$7 < p_{\mathrm{T}} < 8$	$1.01 \pm 0.08 \pm 0.11$
$8 < p_{\mathrm{T}} < 10$	$0.95 \pm 0.09 \pm 0.13$
$10 < p_{\mathrm{T}} < 14$	$0.63 \pm 0.08 \pm 0.09$

Table 28. Double ratio $R^{p\mathrm{Pb}}_{\psi(2S)/J/\psi}$ in pPb collisions for prompt production, as a function of p_{T}, integrated over y^*. The first uncertainty is statistical and the second systematic.

p_{T} interval (GeV/c)	$R^{p\mathrm{Pb}}_{\psi(2S)/J/\psi}$
$0 < p_{\mathrm{T}} < 1$	$0.64 \pm 0.13 \pm 0.27$
$1 < p_{\mathrm{T}} < 2$	$0.82 \pm 0.07 \pm 0.18$
$2 < p_{\mathrm{T}} < 3$	$0.77 \pm 0.07 \pm 0.14$
$3 < p_{\mathrm{T}} < 4$	$0.82 \pm 0.07 \pm 0.17$
$4 < p_{\mathrm{T}} < 5$	$0.69 \pm 0.06 \pm 0.13$
$5 < p_{\mathrm{T}} < 6$	$0.79 \pm 0.07 \pm 0.12$
$6 < p_{\mathrm{T}} < 7$	$0.81 \pm 0.07 \pm 0.13$
$7 < p_{\mathrm{T}} < 8$	$0.76 \pm 0.08 \pm 0.12$
$8 < p_{\mathrm{T}} < 10$	$1.13 \pm 0.11 \pm 0.15$
$10 < p_{\mathrm{T}} < 14$	$0.88 \pm 0.11 \pm 0.14$

Table 29. Double ratio $R^{p\mathrm{Pb}}_{\psi(2S)/J/\psi}$ in Pbp collisions for prompt production, as a function of p_{T}, integrated over y^*. The first uncertainty is statistical and the second systematic.

JHEP04(2024)111

p_{T} interval (GeV/c)	$R^{p\mathrm{Pb}}_{\psi(2S)/J/\psi}$
$0 < p_{\mathrm{T}} < 1$	$1.18 \pm 0.25 \pm 0.21$
$1 < p_{\mathrm{T}} < 2$	$0.91 \pm 0.11 \pm 0.12$
$2 < p_{\mathrm{T}} < 3$	$0.94 \pm 0.11 \pm 0.11$
$3 < p_{\mathrm{T}} < 4$	$1.15 \pm 0.10 \pm 0.12$
$4 < p_{\mathrm{T}} < 5$	$0.99 \pm 0.10 \pm 0.10$
$5 < p_{\mathrm{T}} < 6$	$1.11 \pm 0.11 \pm 0.12$
$6 < p_{\mathrm{T}} < 7$	$1.26 \pm 0.14 \pm 0.14$
$7 < p_{\mathrm{T}} < 8$	$0.83 \pm 0.14 \pm 0.12$
$8 < p_{\mathrm{T}} < 10$	$1.27 \pm 0.16 \pm 0.16$
$10 < p_{\mathrm{T}} < 14$	$1.31 \pm 0.18 \pm 0.20$

Table 30. Double ratio $R^{p\mathrm{Pb}}_{\psi(2S)/J/\psi}$ in pPb collisions for nonprompt production, as a function of p_{T}, integrated over y^*. The first uncertainty is statistical and the second systematic.

p_{T} interval (GeV/c)	$R^{p\mathrm{Pb}}_{\psi(2S)/J/\psi}$
$0 < p_{\mathrm{T}} < 1$	$1.34 \pm 0.31 \pm 0.24$
$1 < p_{\mathrm{T}} < 2$	$0.99 \pm 0.12 \pm 0.14$
$2 < p_{\mathrm{T}} < 3$	$1.11 \pm 0.12 \pm 0.14$
$3 < p_{\mathrm{T}} < 4$	$1.49 \pm 0.13 \pm 0.17$
$4 < p_{\mathrm{T}} < 5$	$1.17 \pm 0.11 \pm 0.13$
$5 < p_{\mathrm{T}} < 6$	$1.07 \pm 0.12 \pm 0.12$
$6 < p_{\mathrm{T}} < 7$	$1.16 \pm 0.15 \pm 0.14$
$7 < p_{\mathrm{T}} < 8$	$1.07 \pm 0.18 \pm 0.15$
$8 < p_{\mathrm{T}} < 10$	$1.08 \pm 0.18 \pm 0.14$
$10 < p_{\mathrm{T}} < 14$	$0.87 \pm 0.17 \pm 0.15$

Table 31. Double ratio $R^{p\mathrm{Pb}}_{\psi(2S)/J/\psi}$ in Pbp collisions for nonprompt production, as a function of p_{T}, integrated over y^*. The first uncertainty is statistical and the second systematic.

JHEP04(2024)111

y^* interval	$R^{p\mathrm{Pb}}_{\psi(2S)/J/\psi}$
$-5.00 < y^* < -4.00$	$0.77 \pm 0.05 \pm 0.10$
$-4.00 < y^* < -3.25$	$0.67 \pm 0.04 \pm 0.10$
$-3.25 < y^* < -2.50$	$0.75 \pm 0.05 \pm 0.11$
$1.50 < y^* < 2.50$	$0.82 \pm 0.05 \pm 0.11$
$2.50 < y^* < 3.25$	$0.80 \pm 0.04 \pm 0.10$
$3.25 < y^* < 4.00$	$0.86 \pm 0.05 \pm 0.11$

Table 32. Double ratio $R^{p\mathrm{Pb}}_{\psi(2S)/J/\psi}$ for prompt production, as a function of y^*, integrated over p_T. The first uncertainty is statistical and the second systematic.

y^* interval	$R^{p\mathrm{Pb}}_{\psi(2S)/J/\psi}$
$-5.00 < y^* < -4.00$	$0.94 \pm 0.11 \pm 0.20$
$-4.00 < y^* < -3.25$	$1.04 \pm 0.08 \pm 0.28$
$-3.25 < y^* < -2.50$	$1.38 \pm 0.11 \pm 0.44$
$1.50 < y^* < 2.50$	$0.97 \pm 0.07 \pm 0.14$
$2.50 < y^* < 3.25$	$1.17 \pm 0.09 \pm 0.16$
$3.25 < y^* < 4.00$	$1.14 \pm 0.11 \pm 0.15$

Table 33. Double ratio $R^{p\mathrm{Pb}}_{\psi(2S)/J/\psi}$ for nonprompt production, as a function of y^*, integrated over p_T. The first uncertainty is statistical and the second systematic.

y^* interval	$R^{p\mathrm{Pb}}_{\psi(2S)/J/\psi}$
$-5.00 < y^* < -2.50$	$0.73 \pm 0.03 \pm 0.06$
$1.50 < y^* < 4.00$	$0.82 \pm 0.03 \pm 0.07$

Table 34. Double ratio $R^{p\mathrm{Pb}}_{\psi(2S)/J/\psi}$ for prompt production, integrated over p_T and y^*. The first uncertainty is statistical and the second systematic.

y^* interval	$R^{p\mathrm{Pb}}_{\psi(2S)/J/\psi}$
$-5.00 < y^* < -2.50$	$1.17 \pm 0.07 \pm 0.11$
$1.50 < y^* < 4.00$	$1.06 \pm 0.06 \pm 0.10$

Table 35. Double ratio $R^{p\mathrm{Pb}}_{\psi(2S)/J/\psi}$ for nonprompt production, integrated over p_T and y^*. The first uncertainty is statistical and the second systematic.

JHEP04(2024)111

References

[1] T. Matsui and H. Satz, *J/ψ suppression by quark-gluon plasma formation*, *Phys. Lett. B* **178** (1986) 416 [INSPIRE].

[2] A. Mocsy, P. Petreczky and M. Strickland, *Quarkonia in the quark gluon plasma*, *Int. J. Mod. Phys. A* **28** (2013) 1340012 [arXiv:1302.2180] [INSPIRE].

[3] A. Andronic et al., *Heavy-flavour and quarkonium production in the LHC era: from proton-proton to heavy-ion collisions*, *Eur. Phys. J. C* **76** (2016) 107 [arXiv:1506.03981] [INSPIRE].

[4] ALICE collaboration, *J/ψ suppression at forward rapidity in Pb-Pb collisions at $\sqrt{s_{\rm NN}} = 2.76$ TeV*, *Phys. Rev. Lett.* **109** (2012) 072301 [arXiv:1202.1383] [INSPIRE].

[5] ALICE collaboration, *Centrality, rapidity and transverse momentum dependence of J/ψ suppression in Pb-Pb collisions at $\sqrt{s_{\rm NN}} = 2.76$ TeV*, *Phys. Lett. B* **734** (2014) 314 [arXiv:1311.0214] [INSPIRE].

[6] ALICE collaboration, *Inclusive, prompt and non-prompt J/ψ production at mid-rapidity in Pb-Pb collisions at $\sqrt{s_{\rm NN}} = 2.76$ TeV*, *JHEP* **07** (2015) 051 [arXiv:1504.07151] [INSPIRE].

[7] ALICE collaboration, *Differential studies of inclusive J/ψ and $\psi(2S)$ production at forward rapidity in Pb-Pb collisions at $\sqrt{s_{\rm NN}} = 2.76$ TeV*, *JHEP* **05** (2016) 179 [arXiv:1506.08804] [INSPIRE].

[8] ALICE collaboration, *J/ψ suppression at forward rapidity in Pb-Pb collisions at $\sqrt{s_{\rm NN}} = 5.02$ TeV*, *Phys. Lett. B* **766** (2017) 212 [arXiv:1606.08197] [INSPIRE].

[9] R.L. Thews, M. Schroedter and J. Rafelski, *Enhanced J/ψ production in deconfined quark matter*, *Phys. Rev. C* **63** (2001) 054905 [hep-ph/0007323] [INSPIRE].

[10] P. Braun-Munzinger and J. Stachel, *(Non)thermal aspects of charmonium production and a new look at J/ψ suppression*, *Phys. Lett. B* **490** (2000) 196 [nucl-th/0007059] [INSPIRE].

[11] H. Satz, *Colour deconfinement and quarkonium binding*, *J. Phys. G* **32** (2006) R25 [hep-ph/0512217] [INSPIRE].

[12] ALICE collaboration, *Upgrade of the ALICE experiment: letter of intent*, *J. Phys. G* **41** (2014) 087001 [INSPIRE].

[13] CMS collaboration, *Measurement of prompt $\psi(2S) \to J/\psi$ yield ratios in Pb-Pb and p-p collisions at $\sqrt{s_{\rm NN}} = 2.76$ TeV*, *Phys. Rev. Lett.* **113** (2014) 262301 [arXiv:1410.1804] [INSPIRE].

[14] CMS collaboration, *Measurement of prompt and nonprompt charmonium suppression in PbPb collisions at 5.02 TeV*, *Eur. Phys. J. C* **78** (2018) 509 [*Erratum ibid.* **83** (2023) 145] [arXiv:1712.08959] [INSPIRE].

[15] CMS collaboration, *Relative modification of prompt $\psi(2S)$ and J/ψ yields from pp to PbPb collisions at $\sqrt{s_{\rm NN}} = 5.02$ TeV*, *Phys. Rev. Lett.* **118** (2017) 162301 [arXiv:1611.01438] [INSPIRE].

JHEP04(2024)111

[16] ALICE collaboration, *$\psi(2S)$ suppression in Pb-Pb collisions at the LHC*, *Phys. Rev. Lett.* **132** (2024) 042301 [arXiv:2210.08893] [INSPIRE].

[17] ATLAS collaboration, *Prompt and non-prompt J/ψ and $\psi(2S)$ suppression at high transverse momentum in 5.02 TeV Pb+Pb collisions with the ATLAS experiment*, *Eur. Phys. J. C* **78** (2018) 762 [arXiv:1805.04077] [INSPIRE].

[18] D. de Florian, R. Sassot, P. Zurita and M. Stratmann, *Global analysis of nuclear parton distributions*, *Phys. Rev. D* **85** (2012) 074028 [arXiv:1112.6324] [INSPIRE].

[19] K. Kovarik et al., *nCTEQ15 — global analysis of nuclear parton distributions with uncertainties in the CTEQ framework*, *Phys. Rev. D* **93** (2016) 085037 [arXiv:1509.00792] [INSPIRE].

[20] K.J. Eskola, P. Paakkinen, H. Paukkunen and C.A. Salgado, *EPPS21: a global QCD analysis of nuclear PDFs*, *Eur. Phys. J. C* **82** (2022) 413 [arXiv:2112.12462] [INSPIRE].

[21] R. Abdul Khalek et al., *nNNPDF3.0: evidence for a modified partonic structure in heavy nuclei*, *Eur. Phys. J. C* **82** (2022) 507 [arXiv:2201.12363] [INSPIRE].

[22] P. Duwentäster et al., *Impact of heavy quark and quarkonium data on nuclear gluon PDFs*, *Phys. Rev. D* **105** (2022) 114043 [arXiv:2204.09982] [INSPIRE].

[23] F. Gelis, E. Iancu, J. Jalilian-Marian and R. Venugopalan, *The color glass condensate*, *Ann. Rev. Nucl. Part. Sci.* **60** (2010) 463 [arXiv:1002.0333] [INSPIRE].

[24] H. Fujii, F. Gelis and R. Venugopalan, *Quark pair production in high energy pA collisions: general features*, *Nucl. Phys. A* **780** (2006) 146 [hep-ph/0603099] [INSPIRE].

[25] F. Arleo and S. Peigne, *Heavy-quarkonium suppression in p-A collisions from parton energy loss in cold QCD matter*, *JHEP* **03** (2013) 122 [arXiv:1212.0434] [INSPIRE].

[26] R. Vogt, *Shadowing and absorption effects on J/ψ production in dA collisions*, *Phys. Rev. C* **71** (2005) 054902 [hep-ph/0411378] [INSPIRE].

[27] R. Vogt, *Cold nuclear matter effects on J/ψ and Υ production at the LHC*, *Phys. Rev. C* **81** (2010) 044903 [arXiv:1003.3497] [INSPIRE].

[28] J.-P. Lansberg and H.-S. Shao, *Towards an automated tool to evaluate the impact of the nuclear modification of the gluon density on quarkonium, D and B meson production in proton-nucleus collisions*, *Eur. Phys. J. C* **77** (2017) 1 [arXiv:1610.05382] [INSPIRE].

[29] Y.-Q. Ma, R. Venugopalan and H.-F. Zhang, *J/ψ production and suppression in high energy proton-nucleus collisions*, *Phys. Rev. D* **92** (2015) 071901 [arXiv:1503.07772] [INSPIRE].

[30] B. Ducloué, T. Lappi and H. Mäntysaari, *Forward J/ψ production in proton-nucleus collisions at high energy*, *Phys. Rev. D* **91** (2015) 114005 [arXiv:1503.02789] [INSPIRE].

[31] ALICE collaboration, *J/ψ production and nuclear effects in p-Pb collisions at $\sqrt{s_{\rm NN}} = 5.02$ TeV*, *JHEP* **02** (2014) 073 [arXiv:1308.6726] [INSPIRE].

[32] LHCb collaboration, *Study of J/ψ production and cold nuclear matter effects in pPb collisions at $\sqrt{s_{\rm NN}} = 5$ TeV*, *JHEP* **02** (2014) 072 [arXiv:1308.6729] [INSPIRE].

[33] ALICE collaboration, *Rapidity and transverse-momentum dependence of the inclusive J/ψ nuclear modification factor in p-Pb collisions at $\sqrt{s_{\rm NN}} = 5.02$ TeV*, *JHEP* **06** (2015) 055 [arXiv:1503.07179] [INSPIRE].

[34] ALICE collaboration, *Centrality dependence of inclusive J/ψ production in p-Pb collisions at $\sqrt{s_{\rm NN}} = 5.02$ TeV*, *JHEP* **11** (2015) 127 [arXiv:1506.08808] [INSPIRE].

JHEP04(2024)111

[35] ATLAS collaboration, *Measurement of differential J/ψ production cross sections and forward-backward ratios in p+Pb collisions with the ATLAS detector*, Phys. Rev. C **92** (2015) 034904 [arXiv:1505.08141] [INSPIRE].

[36] CMS collaboration, *Measurement of prompt and nonprompt J/ψ production in p-p and p-Pb collisions at $\sqrt{s_{\rm NN}} = 5.02$ TeV*, Eur. Phys. J. C **77** (2017) 269 [arXiv:1702.01462] [INSPIRE].

[37] LHCb collaboration, *Prompt and nonprompt J/ψ production and nuclear modification in p-Pb collisions at $\sqrt{s_{NN}} = 8.16$ TeV*, Phys. Lett. B **774** (2017) 159 [arXiv:1706.07122] [INSPIRE].

[38] PHENIX collaboration, *Nuclear modification of ψ', χ_c, and J/ψ production in d+Au collisions at $\sqrt{s_{\rm NN}} = 200$ GeV*, Phys. Rev. Lett. **111** (2013) 202301 [arXiv:1305.5516] [INSPIRE].

[39] PHENIX collaboration, *Measurement of the relative yields of $\psi(2S)$ to $\psi(1S)$ mesons produced at forward and backward rapidity in p+p, p+Al, p+Au, and ^{3}He+Au collisions at $\sqrt{s_{\rm NN}} = 200$ GeV*, Phys. Rev. C **95** (2017) 034904 [arXiv:1609.06550] [INSPIRE].

[40] ALICE collaboration, *Suppression of $\psi(2S)$ production in p-Pb collisions at $\sqrt{s_{\rm NN}} = 5.02$ TeV*, JHEP **12** (2014) 073 [arXiv:1405.3796] [INSPIRE].

[41] ALICE collaboration, *Centrality dependence of $\psi(2S)$ suppression in p-Pb collisions at $\sqrt{s_{\rm NN}} = 5.02$ TeV*, JHEP **06** (2016) 050 [arXiv:1603.02816] [INSPIRE].

[42] ALICE collaboration, *Measurement of nuclear effects on $\psi(2S)$ production in p-Pb collisions at $\sqrt{s_{\rm NN}} = 8.16$ TeV*, JHEP **07** (2020) 237 [arXiv:2003.06053] [INSPIRE].

[43] ALICE collaboration, *Centrality dependence of J/ψ and $\psi(2S)$ production and nuclear modification in p-Pb collisions at $\sqrt{s_{\rm NN}} = 8.16$ TeV*, JHEP **02** (2021) 002 [arXiv:2008.04806] [INSPIRE].

[44] CMS collaboration, *Measurement of prompt $\psi(2S)$ production cross sections in proton-lead and proton-proton collisions at $\sqrt{s_{\rm NN}} = 5.02$ TeV*, Phys. Lett. B **790** (2019) 509 [arXiv:1805.02248] [INSPIRE].

[45] LHCb collaboration, *Study of $\psi(2S)$ production and cold nuclear matter effects in pPb collisions at $\sqrt{s_{\rm NN}} = 5$ TeV*, JHEP **03** (2016) 133 [arXiv:1601.07878] [INSPIRE].

[46] E.G. Ferreiro, *Excited charmonium suppression in proton-nucleus collisions as a consequence of comovers*, Phys. Lett. B **749** (2015) 98 [arXiv:1411.0549] [INSPIRE].

[47] Y.-Q. Ma, R. Venugopalan, K. Watanabe and H.-F. Zhang, *$\psi(2S)$ versus J/ψ suppression in proton-nucleus collisions from factorization violating soft color exchanges*, Phys. Rev. C **97** (2018) 014909 [arXiv:1707.07266] [INSPIRE].

[48] LHCb collaboration, *The LHCb detector at the LHC*, 2008 JINST **3** S08005 [INSPIRE].

[49] LHCb collaboration, *LHCb detector performance*, Int. J. Mod. Phys. A **30** (2015) 1530022 [arXiv:1412.6352] [INSPIRE].

[50] R. Aaij et al., *Performance of the LHCb vertex locator*, 2014 JINST **9** P09007 [arXiv:1405.7808] [INSPIRE].

[51] LHCb Outer Tracker Group collaboration, *Performance of the LHCb outer tracker*, 2014 JINST **9** P01002 [arXiv:1311.3893] [INSPIRE].

[52] LHCb RICH Group collaboration, *Performance of the LHCb RICH detector at the LHC*, Eur. Phys. J. C **73** (2013) 2431 [arXiv:1211.6759] [INSPIRE].

[53] A.A. Alves Jr. et al., *Performance of the LHCb muon system*, 2013 JINST **8** P02022 [arXiv:1211.1346] [INSPIRE].

JHEP04(2024)111

[54] LHCb collaboration, *Precision luminosity measurements at LHCb*, 2014 *JINST* **9** P12005 [arXiv:1410.0149] [INSPIRE].

[55] PARTICLE DATA GROUP collaboration, *Review of particle physics*, *PTEP* **2022** (2022) 083C01 [INSPIRE].

[56] LHCb collaboration, *Measurement of $\psi(2S)$ production cross-sections in proton-proton collisions at $\sqrt{s} = 7$ and 13 TeV*, *Eur. Phys. J. C* **80** (2020) 185 [arXiv:1908.03099] [INSPIRE].

[57] T. Skwarnicki, *A study of the radiative CASCADE transitions between the Upsilon-Prime and Upsilon resonances*, Ph.D. thesis, INP, Cracow, Poland (1986) [INSPIRE].

[58] T. Pierog et al., *EPOS LHC: test of collective hadronization with data measured at the CERN Large Hadron Collider*, *Phys. Rev. C* **92** (2015) 034906 [arXiv:1306.0121] [INSPIRE].

[59] T. Sjostrand, S. Mrenna and P.Z. Skands, *A brief introduction to PYTHIA* 8.1, *Comput. Phys. Commun.* **178** (2008) 852 [arXiv:0710.3820] [INSPIRE].

[60] D.J. Lange, *The EvtGen particle decay simulation package*, *Nucl. Instrum. Meth. A* **462** (2001) 152 [INSPIRE].

[61] P. Golonka and Z. Was, *PHOTOS Monte Carlo: a precision tool for QED corrections in Z and W decays*, *Eur. Phys. J. C* **45** (2006) 97 [hep-ph/0506026] [INSPIRE].

[62] J. Allison et al., *GEANT4 developments and applications*, *IEEE Trans. Nucl. Sci.* **53** (2006) 270 [INSPIRE].

[63] GEANT4 collaboration, *GEANT4 — a simulation toolkit*, *Nucl. Instrum. Meth. A* **506** (2003) 250 [INSPIRE].

[64] LHCb collaboration, *The LHCb simulation application, Gauss: design, evolution and experience*, *J. Phys. Conf. Ser.* **331** (2011) 032023 [INSPIRE].

[65] LHCb collaboration, *Measurement of the track reconstruction efficiency at LHCb*, 2015 *JINST* **10** P02007 [arXiv:1408.1251] [INSPIRE].

[66] LHCb collaboration, *The PIDCalib package*, LHCb-PUB-2016-021, CERN, Geneva, Switzerland (2016).

[67] ALICE collaboration, *Measurement of the inclusive J/ψ polarization at forward rapidity in pp collisions at $\sqrt{s} = 8$ TeV*, *Eur. Phys. J. C* **78** (2018) 562 [arXiv:1805.04374] [INSPIRE].

[68] LHCb collaboration, *Measurement of J/ψ polarization in pp collisions at $\sqrt{s} = 7$ TeV*, *Eur. Phys. J. C* **73** (2013) 2631 [arXiv:1307.6379] [INSPIRE].

[69] LHCb collaboration, *Measurement of $\psi(2S)$ polarisation in pp collisions at $\sqrt{s} = 7$ TeV*, *Eur. Phys. J. C* **74** (2014) 2872 [arXiv:1403.1339] [INSPIRE].

[70] R. Aaij et al., *The LHCb trigger and its performance in* 2011, 2013 *JINST* **8** P04022 [arXiv:1211.3055] [INSPIRE].

[71] ALICE collaboration, *Measurement of $\psi(2S)$ production as a function of charged-particle pseudorapidity density in pp collisions at $\sqrt{s} = 13$ TeV and p-Pb collisions at $\sqrt{s_{\rm NN}} = 8.16$ TeV with ALICE at the LHC*, *JHEP* **06** (2023) 147 [arXiv:2204.10253] [INSPIRE].

[72] H.-S. Shao, *HELAC-Onia* 2.0*: an upgraded matrix-element and event generator for heavy quarkonium physics*, *Comput. Phys. Commun.* **198** (2016) 238 [arXiv:1507.03435] [INSPIRE].

[73] H.-S. Shao, *HELAC-Onia: an automatic matrix element generator for heavy quarkonium physics*, *Comput. Phys. Commun.* **184** (2013) 2562 [arXiv:1212.5293] [INSPIRE].

JHEP04(2024)111

The LHCb collaboration

R. Aaij[36], A.S.W. Abdelmotteleb[55], C. Abellan Beteta[49], F. Abudinén[55], T. Ackernley[59], B. Adeva[45], M. Adinolfi[53], P. Adlarson[79], H. Afsharnia[11], C. Agapopoulou[47], C.A. Aidala[80], Z. Ajaltouni[11], S. Akar[64], K. Akiba[36], P. Albicocco[26], J. Albrecht[18], F. Alessio[47], M. Alexander[58], A. Alfonso Albero[44], Z. Aliouche[61], P. Alvarez Cartelle[54], R. Amalric[16], S. Amato[3], J.L. Amey[53], Y. Amhis[14,47], L. An[6], L. Anderlini[25], M. Andersson[49], A. Andreianov[42], P. Andreola[49], M. Andreotti[24], D. Andreou[67], A. Anelli[29,n], D. Ao[7], F. Archilli[35,t], S. Arguedas Cuendis[9], A. Artamonov[42], M. Artuso[67], E. Aslanides[12], M. Atzeni[63], B. Audurier[15], D. Bacher[62], I. Bachiller Perea[10], S. Bachmann[20], M. Bachmayer[48], J.J. Back[55], A. Bailly-reyre[16], P. Baladron Rodriguez[45], V. Balagura[15], W. Baldini[24], J. Baptista de Souza Leite[2], M. Barbetti[25,k], I. R. Barbosa[68], R.J. Barlow[61], S. Barsuk[14], W. Barter[57], M. Bartolini[54], F. Baryshnikov[42], J.M. Basels[17], G. Bassi[33,q], B. Batsukh[5], A. Battig[18], A. Bay[48], A. Beck[55], M. Becker[18], F. Bedeschi[33], I.B. Bediaga[2], A. Beiter[67], S. Belin[45], V. Bellee[49], K. Belous[42], I. Belov[27], I. Belyaev[42], G. Benane[12], G. Bencivenni[26], E. Ben-Haim[16], A. Berezhnoy[42], R. Bernet[49], S. Bernet Andres[43], H.C. Bernstein[67], C. Bertella[61], A. Bertolin[31], C. Betancourt[49], F. Betti[57], J. Bex[54], Ia. Bezshyiko[49], J. Bhom[39], M.S. Bieker[18], N.V. Biesuz[24], P. Billoir[16], A. Biolchini[36], M. Birch[60], F.C.R. Bishop[10], A. Bitadze[61], A. Bizzeti[], M.P. Blago[54], T. Blake[55], F. Blanc[48], J.E. Blank[18], S. Blusk[67], D. Bobulska[58], V. Bocharnikov[42], J.A. Boelhauve[18], O. Boente Garcia[15], T. Boettcher[64], A. Bohare[57], A. Boldyrev[42], C.S. Bolognani[77], R. Bolzonella[24,j], N. Bondar[42], F. Borgato[31,47], S. Borghi[61], M. Borsato[29,n], J.T. Borsuk[39], F. Bossù[13], S.A. Bouchiba[48], T.J.V. Bowcock[59], A. Boyer[47], C. Bozzi[24], M.J. Bradley[60], S. Braun[65], A. Brea Rodriguez[45], N. Breer[18], J. Brodzicka[39], A. Brossa Gonzalo[45], J. Brown[59], D. Brundu[30], A. Buonaura[49], L. Buonincontri[31], A.T. Burke[61], C. Burr[47], A. Bursche[70], A. Butkevich[42], J.S. Butter[54], J. Buytaert[47], W. Byczynski[47], S. Cadeddu[30], H. Cai[72], R. Calabrese[24,j], L. Calefice[18], S. Cali[26], M. Calvi[29,n], M. Calvo Gomez[43], J. Cambon Bouzas[45], P. Campana[26], D.H. Campora Perez[77], A.F. Campoverde Quezada[7], S. Capelli[29,n], L. Capriotti[24], A. Carbone[23,h], L. Carcedo Salgado[45], R. Cardinale[27,l], A. Cardini[30], P. Carniti[29,n], L. Carus[20], A. Casais Vidal[63], R. Caspary[20], G. Casse[59], J. Castro Godinez[9], M. Cattaneo[47], G. Cavallero[24], V. Cavallini[24,j], S. Celani[48], J. Cerasoli[12], D. Cervenkov[62], S. Cesare[28,m], A.J. Chadwick[59], I. Chahrour[80], M. Charles[16], Ph. Charpentier[47], C.A. Chavez Barajas[59], M. Chefdeville[10], C. Chen[12], S. Chen[5], A. Chernov[39], S. Chernyshenko[51], V. Chobanova[45,x], S. Cholak[48], M. Chrzaszcz[39], A. Chubykin[42], V. Chulikov[42], P. Ciambrone[26], M.F. Cicala[55], X. Cid Vidal[45], G. Ciezarek[47], P. Cifra[47], P.E.L. Clarke[57], M. Clemencic[47], H.V. Cliff[54], J. Closier[47], J.L. Cobbledick[61], C. Cocha Toapaxi[20], V. Coco[47], J. Cogan[12], E. Cogneras[11], L. Cojocariu[41], P. Collins[47], T. Colombo[47], A. Comerma-Montells[44], L. Congedo[22], A. Contu[30], N. Cooke[58], I. Corredoira[45], A. Correia[16], G. Corti[47], J.J. Cottee Meldrum[53], B. Couturier[47], D.C. Craik[49], M. Cruz Torres[2,f], R. Currie[57], C.L. Da Silva[66], S. Dadabaev[42], L. Dai[69], X. Dai[6], E. Dall'Occo[18], J. Dalseno[45], C. D'Ambrosio[47], J. Daniel[11], A. Danilina[42], P. d'Argent[22], A. Davidson[55], J.E. Davies[61], A. Davis[61],

JHEP04(2024)111

O. De Aguiar Francisco[61], C. De Angelis[30,i], J. de Boer[36], K. De Bruyn[76], S. De Capua[61], M. De Cian[20], U. De Freitas Carneiro Da Graca[2,b], E. De Lucia[26], J.M. De Miranda[2], L. De Paula[3], M. De Serio[22,g], D. De Simone[49], P. De Simone[26], F. De Vellis[18], J.A. de Vries[77], F. Debernardis[22,g], D. Decamp[10], V. Dedu[12], L. Del Buono[16], B. Delaney[63], H.-P. Dembinski[18], J. Deng[8], V. Denysenko[49], O. Deschamps[11], F. Dettori[30,i], B. Dey[75], P. Di Nezza[26], I. Diachkov[42], S. Didenko[42], S. Ding[67], V. Dobishuk[51], A. D. Docheva[58], A. Dolmatov[42], C. Dong[4], A.M. Donohoe[21], F. Dordei[30], A.C. dos Reis[2], L. Douglas[58], A.G. Downes[10], W. Duan[70], P. Duda[78], M.W. Dudek[39], L. Dufour[47], V. Duk[32], P. Durante[47], M. M. Duras[78], J.M. Durham[66], D. Dutta[61], A. Dziurda[39], A. Dzyuba[42], S. Easo[56,47], E. Eckstein[74], U. Egede[1], A. Egorychev[42], V. Egorychev[42], C. Eirea Orro[45], S. Eisenhardt[57], E. Ejopu[61], S. Ek-In[48], L. Eklund[79], M. Elashri[64], J. Ellbracht[18], S. Ely[60], A. Ene[41], E. Epple[64], S. Escher[17], J. Eschle[49], S. Esen[49], T. Evans[61], F. Fabiano[30,i,47], L.N. Falcao[2], Y. Fan[7], B. Fang[72,14], L. Fantini[32,p], M. Faria[48], K. Farmer[57], D. Fazzini[29,n], L. Felkowski[78], M. Feng[5,7], M. Feo[47], M. Fernandez Gomez[45], A.D. Fernez[65], F. Ferrari[23], F. Ferreira Rodrigues[3], S. Ferreres Sole[36], M. Ferrillo[49], M. Ferro-Luzzi[47], S. Filippov[42], R.A. Fini[22], M. Fiorini[24,j], M. Firlej[38], K.M. Fischer[62], D.S. Fitzgerald[80], C. Fitzpatrick[61], T. Fiutowski[38], F. Fleuret[15], M. Fontana[23], F. Fontanelli[27,l], L. F. Foreman[61], R. Forty[47], D. Foulds-Holt[54], M. Franco Sevilla[65], M. Frank[47], E. Franzoso[24,j], G. Frau[20], C. Frei[47], D.A. Friday[61], L. Frontini[28], J. Fu[7], Q. Fuehring[18], Y. Fujii[1], T. Fulghesu[16], E. Gabriel[36], G. Galati[22,g], M.D. Galati[36], A. Gallas Torreira[45], D. Galli[23,h], S. Gambetta[57,47], M. Gandelman[3], P. Gandini[28], H. Gao[7], R. Gao[62], Y. Gao[8], Y. Gao[6], Y. Gao[8], M. Garau[30,i], L.M. Garcia Martin[48], P. Garcia Moreno[44], J. García Pardiñas[47], B. Garcia Plana[45], K. G. Garg[8], L. Garrido[44], C. Gaspar[47], R.E. Geertsema[36], L.L. Gerken[18], E. Gersabeck[61], M. Gersabeck[61], T. Gershon[55], Z. Ghorbanimoghaddam[53], L. Giambastiani[31], F. I. Giasemis[16,d], V. Gibson[54], H.K. Giemza[40], A.L. Gilman[62], M. Giovannetti[26], A. Gioventù[44], P. Gironella Gironell[44], C. Giugliano[24,j], M.A. Giza[39], E.L. Gkougkousis[60], F.C. Glaser[14,20], V.V. Gligorov[16], C. Göbel[68], E. Golobardes[43], D. Golubkov[42], A. Golutvin[60,42,47], A. Gomes[2,a,†], S. Gomez Fernandez[44], F. Goncalves Abrantes[62], M. Goncerz[39], G. Gong[4], J. A. Gooding[18], I.V. Gorelov[42], C. Gotti[29], J.P. Grabowski[74], L.A. Granado Cardoso[47], E. Graugés[44], E. Graverini[48], L. Grazette[55], G. Graziani[], A. T. Grecu[41], L.M. Greeven[36], N.A. Grieser[64], L. Grillo[58], S. Gromov[42], C. Gu[15], M. Guarise[24], M. Guittiere[14], V. Guliaeva[42], P. A. Günther[20], A.-K. Guseinov[42], E. Gushchin[42], Y. Guz[6,42,47], T. Gys[47], T. Hadavizadeh[1], C. Hadjivasiliou[65], G. Haefeli[48], C. Haen[47], J. Haimberger[47], M. Hajheidari[47], T. Halewood-leagas[59], M.M. Halvorsen[47], P.M. Hamilton[65], J. Hammerich[59], Q. Han[8], X. Han[20], S. Hansmann-Menzemer[20], L. Hao[7], N. Harnew[62], T. Harrison[59], M. Hartmann[14], C. Hasse[47], J. He[7,c], K. Heijhoff[36], F. Hemmer[47], C. Henderson[64], R.D.L. Henderson[1,55], A.M. Hennequin[47], K. Hennessy[59], L. Henry[48], J. Herd[60], J. Heuel[17], A. Hicheur[3], D. Hill[48], S.E. Hollitt[18], J. Horswill[61], R. Hou[8], Y. Hou[10], N. Howarth[59], J. Hu[20], J. Hu[70], W. Hu[6], X. Hu[4], W. Huang[7], W. Hulsbergen[36], R.J. Hunter[55], M. Hushchyn[42], D. Hutchcroft[59], M. Idzik[38], D. Ilin[42], P. Ilten[64], A. Inglessi[42], A. Iniukhin[42],

A. Ishteev[42], K. Ivshin[42], R. Jacobsson[47], H. Jage[17], S.J. Jaimes Elles[46,73], S. Jakobsen[47], E. Jans[36], B.K. Jashal[46], A. Jawahery[65], V. Jevtic[18], E. Jiang[65], X. Jiang[5,7], Y. Jiang[7], Y. J. Jiang[6], M. John[62], D. Johnson[52], C.R. Jones[54], T.P. Jones[55], S. Joshi[40], B. Jost[47], N. Jurik[47], I. Juszczak[39], D. Kaminaris[48], S. Kandybei[50], Y. Kang[4], M. Karacson[47], D. Karpenkov[42], M. Karpov[42], A. M. Kauniskangas[48], J.W. Kautz[64], F. Keizer[47], D.M. Keller[67], M. Kenzie[54], T. Ketel[36], B. Khanji[67], A. Kharisova[42], S. Kholodenko[33], G. Khreich[14], T. Kirn[17], V.S. Kirsebom[48], O. Kitouni[63], S. Klaver[37], N. Kleijne[33,q], K. Klimaszewski[40], M.R. Kmiec[40], S. Koliiev[51], L. Kolk[18], A. Konoplyannikov[42], P. Kopciewicz[38,47], P. Koppenburg[36], M. Korolev[42], I. Kostiuk[36], O. Kot[51], S. Kotriakhova, A. Kozachuk[42], P. Kravchenko[42], L. Kravchuk[42], M. Kreps[55], S. Kretzschmar[17], P. Krokovny[42], W. Krupa[67], W. Krzemien[40], J. Kubat[20], S. Kubis[78], W. Kucewicz[39], M. Kucharczyk[39], V. Kudryavtsev[42], E. Kulikova[42], A. Kupsc[79], B. K. Kutsenko[12], D. Lacarrere[47], G. Lafferty[61], A. Lai[30], A. Lampis[30], D. Lancierini[49], C. Landesa Gomez[45], J.J. Lane[1], R. Lane[53], C. Langenbruch[20], J. Langer[18], O. Lantwin[42], T. Latham[55], F. Lazzari[33,r], C. Lazzeroni[52], R. Le Gac[12], S.H. Lee[80], R. Lefèvre[11], A. Leflat[42], S. Legotin[42], M. Lehuraux[55], O. Leroy[12], T. Lesiak[39], B. Leverington[20], A. Li[4], H. Li[70], K. Li[8], L. Li[61], P. Li[47], P.-R. Li[71], S. Li[8], T. Li[5], T. Li[70], Y. Li[8], Y. Li[5], Z. Li[67], Z. Lian[4], X. Liang[67], C. Lin[7], T. Lin[56], R. Lindner[47], V. Lisovskyi[48], R. Litvinov[30,i], G. Liu[70], H. Liu[7], K. Liu[71], Q. Liu[7], S. Liu[5,7], Y. Liu[57], Y. Liu[71], Y. L. Liu[60], A. Lobo Salvia[44], A. Loi[30], J. Lomba Castro[45], T. Long[54], J.H. Lopes[3], A. Lopez Huertas[44], S. López Soliño[45], G.H. Lovell[54], C. Lucarelli[25,k], D. Lucchesi[31,o], S. Luchuk[42], M. Lucio Martinez[77], V. Lukashenko[36,51], Y. Luo[6], A. Lupato[31], E. Luppi[24,j], K. Lynch[21], X.-R. Lyu[7], G. M. Ma[4], R. Ma[7], S. Maccolini[18], F. Machefert[14], F. Maciuc[41], I. Mackay[62], L.R. Madhan Mohan[54], M. M. Madurai[52], A. Maevskiy[42], D. Magdalinski[36], D. Maisuzenko[42], M.W. Majewski[38], J.J. Malczewski[39], S. Malde[62], B. Malecki[39,47], L. Malentacca[47], A. Malinin[42], T. Maltsev[42], G. Manca[30,i], G. Mancinelli[12], C. Mancuso[28,14,m], R. Manera Escalero[44], D. Manuzzi[23], D. Marangotto[28,m], J.F. Marchand[10], R. Marchevski[48], U. Marconi[23], S. Mariani[47], C. Marin Benito[44,47], J. Marks[20], A.M. Marshall[53], P.J. Marshall[59], G. Martelli[32,p], G. Martellotti[34], L. Martinazzoli[47], M. Martinelli[29,n], D. Martinez Santos[45], F. Martinez Vidal[46], A. Massafferri[2], M. Materok[17], R. Matev[47], A. Mathad[49], V. Matiunin[42], C. Matteuzzi[67,29], K.R. Mattioli[15], A. Mauri[60], E. Maurice[15], J. Mauricio[44], M. Mazurek[47], M. McCann[60], L. Mcconnell[21], T.H. McGrath[61], N.T. McHugh[58], A. McNab[61], R. McNulty[21], B. Meadows[64], G. Meier[18], D. Melnychuk[40], M. Merk[36,77], A. Merli[28,m], L. Meyer Garcia[3], D. Miao[5,7], H. Miao[7], M. Mikhasenko[74,e], D.A. Milanes[73], A. Minotti[29,n], E. Minucci[67], T. Miralles[11], S.E. Mitchell[57], B. Mitreska[18], D.S. Mitzel[18], A. Modak[56], A. Mödden[18], R.A. Mohammed[62], R.D. Moise[17], S. Mokhnenko[42], T. Mombächer[47], M. Monk[55,1], I.A. Monroy[73], S. Monteil[11], A. Morcillo Gomez[45], G. Morello[26], M.J. Morello[33,q], M.P. Morgenthaler[20], J. Moron[38], A.B. Morris[47], A.G. Morris[12], R. Mountain[67], H. Mu[4], Z. M. Mu[6], E. Muhammad[55], F. Muheim[57], M. Mulder[76], K. Müller[49], F. Muñoz-Rojas[9], R. Murta[60], P. Naik[59], T. Nakada[48], R. Nandakumar[56], T. Nanut[47],

JHEP04(2024)111

I. Nasteva[3], M. Needham[57], N. Neri[28,m], S. Neubert[74], N. Neufeld[47], P. Neustroev[42], R. Newcombe[60], J. Nicolini[18,14], D. Nicotra[77], E.M. Niel[48], N. Nikitin[42], P. Nogga[74], N.S. Nolte[63], C. Normand[10,i,30], J. Novoa Fernandez[45], G. Nowak[64], C. Nunez[80], H. N. Nur[58], A. Oblakowska-Mucha[38], V. Obraztsov[42], T. Oeser[17], S. Okamura[24,j,47], R. Oldeman[30,i], F. Oliva[57], M. Olocco[18], C.J.G. Onderwater[77], R.H. O'Neil[57], J.M. Otalora Goicochea[3], T. Ovsiannikova[42], P. Owen[49], A. Oyanguren[46], O. Ozcelik[57], K.O. Padeken[74], B. Pagare[55], P.R. Pais[20], T. Pajero[62], A. Palano[22], M. Palutan[26], G. Panshin[42], L. Paolucci[55], A. Papanestis[56], M. Pappagallo[22,g], L.L. Pappalardo[24,j], C. Pappenheimer[64], C. Parkes[61], B. Passalacqua[24,j], G. Passaleva[25], D. Passaro[33,q], A. Pastore[22], M. Patel[60], J. Patoc[62], C. Patrignani[23,h], C.J. Pawley[77], A. Pellegrino[36], M. Pepe Altarelli[26], S. Perazzini[23], D. Pereima[42], A. Pereiro Castro[45], P. Perret[11], A. Perro[47], K. Petridis[53], A. Petrolini[27,l], S. Petrucci[57], H. Pham[67], L. Pica[33,q], M. Piccini[32], B. Pietrzyk[10], G. Pietrzyk[14], D. Pinci[34], F. Pisani[47], M. Pizzichemi[29,n], V. Placinta[41], M. Plo Casasus[45], F. Polci[16,47], M. Poli Lener[26], A. Poluektov[12], N. Polukhina[42], I. Polyakov[47], E. Polycarpo[3], S. Ponce[47], D. Popov[7], S. Poslavskii[42], K. Prasanth[39], L. Promberger[20], C. Prouve[45], V. Pugatch[51], V. Puill[14], G. Punzi[33,r], H.R. Qi[4], W. Qian[7], N. Qin[4], S. Qu[4], R. Quagliani[48], B. Rachwal[38], J.H. Rademacker[53], M. Rama[33], M. Ramírez García[80], M. Ramos Pernas[55], M.S. Rangel[3], F. Ratnikov[42], G. Raven[37], M. Rebollo De Miguel[46], F. Redi[47], J. Reich[53], F. Reiss[61], Z. Ren[4], P.K. Resmi[62], R. Ribatti[33,q], G. R. Ricart[15,81], D. Riccardi[33,q], S. Ricciardi[56], K. Richardson[63], M. Richardson-Slipper[57], K. Rinnert[59], P. Robbe[14], G. Robertson[57], E. Rodrigues[59,47], E. Rodriguez Fernandez[45], J.A. Rodriguez Lopez[73], E. Rodriguez Rodriguez[45], A. Rogovskiy[56], D.L. Rolf[47], A. Rollings[62], P. Roloff[47], V. Romanovskiy[42], M. Romero Lamas[45], A. Romero Vidal[45], G. Romolini[24], F. Ronchetti[48], M. Rotondo[26], S. R. Roy[20], M.S. Rudolph[67], T. Ruf[47], M. Ruiz Diaz[20], R.A. Ruiz Fernandez[45], J. Ruiz Vidal[79,y], A. Ryzhikov[42], J. Ryzka[38], J.J. Saborido Silva[45], R. Sadek[15], N. Sagidova[42], N. Sahoo[52], B. Saitta[30,i], M. Salomoni[47], C. Sanchez Gras[36], I. Sanderswood[46], R. Santacesaria[34], C. Santamarina Rios[45], M. Santimaria[26], L. Santoro[2], E. Santovetti[35], A. Saputi[24,47], D. Saranin[42], G. Sarpis[57], M. Sarpis[74], A. Sarti[34], C. Satriano[34,s], A. Satta[35], M. Saur[6], D. Savrina[42], H. Sazak[11], L.G. Scantlebury Smead[62], A. Scarabotto[16], S. Schael[17], S. Scherl[59], A. M. Schertz[75], M. Schiller[58], H. Schindler[47], M. Schmelling[19], B. Schmidt[47], S. Schmitt[17], H. Schmitz[74], O. Schneider[48], A. Schopper[47], N. Schulte[18], S. Schulte[48], M.H. Schune[14], R. Schwemmer[47], G. Schwering[17], B. Sciascia[26], A. Sciuccati[47], S. Sellam[45], A. Semennikov[42], M. Senghi Soares[37], A. Sergi[27,l], N. Serra[49,47], L. Sestini[31], A. Seuthe[18], Y. Shang[6], D.M. Shangase[80], M. Shapkin[42], I. Shchemerov[42], L. Shchutska[48], T. Shears[59], L. Shekhtman[42], Z. Shen[6], S. Sheng[5,7], V. Shevchenko[42], B. Shi[7], E.B. Shields[29,n], Y. Shimizu[14], E. Shmanin[42], R. Shorkin[42], J.D. Shupperd[67], R. Silva Coutinho[67], G. Simi[31], S. Simone[22,g], N. Skidmore[61], R. Skuza[20], T. Skwarnicki[67], M.W. Slater[52], J.C. Smallwood[62], E. Smith[63], K. Smith[66], M. Smith[60], A. Snoch[36], L. Soares Lavra[57], M.D. Sokoloff[64], F.J.P. Soler[58], A. Solomin[42,53], A. Solovev[42], I. Solovyev[42], R. Song[1], Y. Song[48], Y. Song[4], Y. S. Song[6], F.L. Souza De Almeida[3], B. Souza De Paula[3], E. Spadaro Norella[28,m], E. Spedicato[23],

JHEP04(2024)111

J.G. Speer[18], E. Spiridenkov[42], P. Spradlin[58], V. Sriskaran[47], F. Stagni[47], M. Stahl[47], S. Stahl[47], S. Stanislaus[62], E.N. Stein[47], O. Steinkamp[49], O. Stenyakin[42], H. Stevens[18], D. Strekalina[42], Y. Su[7], F. Suljik[62], J. Sun[30], L. Sun[72], Y. Sun[65], P.N. Swallow[52], K. Swientek[38], F. Swystun[55], A. Szabelski[40], T. Szumlak[38], M. Szymanski[47], Y. Tan[4], S. Taneja[61], M.D. Tat[62], A. Terentev[49], F. Terzuoli[33,u], F. Teubert[47], E. Thomas[47], D.J.D. Thompson[52], H. Tilquin[60], V. Tisserand[11], S. T'Jampens[10], M. Tobin[5], L. Tomassetti[24,j], G. Tonani[28,m], X. Tong[6], D. Torres Machado[2], L. Toscano[18], D.Y. Tou[4], C. Trippl[43], G. Tuci[20], N. Tuning[36], L.H. Uecker[20], A. Ukleja[38], D.J. Unverzagt[20], E. Ursov[42], A. Usachov[37], A. Ustyuzhanin[42], U. Uwer[20], V. Vagnoni[23], A. Valassi[47], G. Valenti[23], N. Valls Canudas[43], H. Van Hecke[66], E. van Herwijnen[60], C.B. Van Hulse[45,w], R. Van Laak[48], M. van Veghel[36], R. Vazquez Gomez[44], P. Vazquez Regueiro[45], C. Vázquez Sierra[45], S. Vecchi[24], J.J. Velthuis[53], M. Veltri[25,v], A. Venkateswaran[48], M. Vesterinen[55], D. Vieira[64], M. Vieites Diaz[47], X. Vilasis-Cardona[43], E. Vilella Figueras[59], A. Villa[23], P. Vincent[16], F.C. Volle[14], D. vom Bruch[12], V. Vorobyev[42], N. Voropaev[42], K. Vos[77], C. Vrahas[57], J. Walsh[33], E.J. Walton[1], G. Wan[6], C. Wang[20], G. Wang[8], J. Wang[6], J. Wang[5], J. Wang[4], J. Wang[72], M. Wang[28], N. W. Wang[7], R. Wang[53], X. Wang[70], X. W. Wang[60], Y. Wang[8], Z. Wang[14], Z. Wang[4], Z. Wang[7], J.A. Ward[55,1], N.K. Watson[52], D. Websdale[60], Y. Wei[6], B.D.C. Westhenry[53], D.J. White[61], M. Whitehead[58], A.R. Wiederhold[55], D. Wiedner[18], G. Wilkinson[62], M.K. Wilkinson[64], M. Williams[63], M.R.J. Williams[57], R. Williams[54], F.F. Wilson[56], M. Winn[13], W. Wislicki[40], M. Witek[39], L. Witola[20], C.P. Wong[66], G. Wormser[14], S.A. Wotton[54], H. Wu[67], J. Wu[8], Y. Wu[6], K. Wyllie[47], S. Xian[70], Z. Xiang[5], Y. Xie[8], A. Xu[33], J. Xu[7], L. Xu[4], L. Xu[4], M. Xu[55], Z. Xu[11], Z. Xu[7], Z. Xu[5], D. Yang[4], S. Yang[7], X. Yang[6], Y. Yang[27,l], Z. Yang[6], Z. Yang[65], V. Yeroshenko[14], H. Yeung[61], H. Yin[8], C. Y. Yu[6], J. Yu[69], X. Yuan[5], E. Zaffaroni[48], M. Zavertyaev[19], M. Zdybal[39], M. Zeng[4], C. Zhang[6], D. Zhang[8], J. Zhang[7], L. Zhang[4], S. Zhang[69], S. Zhang[6], Y. Zhang[6], Y. Zhang[62], Y. Z. Zhang[4], Y. Zhao[20], A. Zharkova[42], A. Zhelezov[20], X. Z. Zheng[4], Y. Zheng[7], T. Zhou[6], X. Zhou[8], Y. Zhou[7], V. Zhovkovska[14], L. Z. Zhu[7], X. Zhu[4], X. Zhu[8], Z. Zhu[7], V. Zhukov[17,42], J. Zhuo[46], Q. Zou[5,7], D. Zuliani[31], G. Zunica[61]

[1] *School of Physics and Astronomy, Monash University, Melbourne, Australia*
[2] *Centro Brasileiro de Pesquisas Físicas (CBPF), Rio de Janeiro, Brazil*
[3] *Universidade Federal do Rio de Janeiro (UFRJ), Rio de Janeiro, Brazil*
[4] *Center for High Energy Physics, Tsinghua University, Beijing, China*
[5] *Institute Of High Energy Physics (IHEP), Beijing, China*
[6] *School of Physics State Key Laboratory of Nuclear Physics and Technology, Peking University, Beijing, China*
[7] *University of Chinese Academy of Sciences, Beijing, China*
[8] *Institute of Particle Physics, Central China Normal University, Wuhan, Hubei, China*
[9] *Consejo Nacional de Rectores (CONARE), San Jose, Costa Rica*
[10] *Université Savoie Mont Blanc, CNRS, IN2P3-LAPP, Annecy, France*
[11] *Université Clermont Auvergne, CNRS/IN2P3, LPC, Clermont-Ferrand, France*
[12] *Aix Marseille Univ, CNRS/IN2P3, CPPM, Marseille, France*
[13] *LAL, Univ. Paris-Sud, CNRS/IN2P3, Université Paris-Saclay, Orsay, France*
[14] *Université Paris-Saclay, CNRS/IN2P3, IJCLab, Orsay, France*

JHEP04(2024)111

[15] Laboratoire Leprince-Ringuet, CNRS/IN2P3, Ecole Polytechnique, Institut Polytechnique de Paris, Palaiseau, France
[16] LPNHE, Sorbonne Université, Paris Diderot Sorbonne Paris Cité, CNRS/IN2P3, Paris, France
[17] I. Physikalisches Institut, RWTH Aachen University, Aachen, Germany
[18] Fakultät Physik, Technische Universität Dortmund, Dortmund, Germany
[19] Max-Planck-Institut für Kernphysik (MPIK), Heidelberg, Germany
[20] Physikalisches Institut, Ruprecht-Karls-Universität Heidelberg, Heidelberg, Germany
[21] School of Physics, University College Dublin, Dublin, Ireland
[22] INFN Sezione di Bari, Bari, Italy
[23] INFN Sezione di Bologna, Bologna, Italy
[24] INFN Sezione di Ferrara, Ferrara, Italy
[25] INFN Sezione di Firenze, Firenze, Italy
[26] INFN Laboratori Nazionali di Frascati, Frascati, Italy
[27] INFN Sezione di Genova, Genova, Italy
[28] INFN Sezione di Milano, Milano, Italy
[29] INFN Sezione di Milano-Bicocca, Milano, Italy
[30] INFN Sezione di Cagliari, Monserrato, Italy
[31] Università degli Studi di Padova, Università e INFN, Padova, Padova, Italy
[32] INFN Sezione di Perugia, Perugia, Italy
[33] INFN Sezione di Pisa, Pisa, Italy
[34] INFN Sezione di Roma La Sapienza, Roma, Italy
[35] INFN Sezione di Roma Tor Vergata, Roma, Italy
[36] Nikhef National Institute for Subatomic Physics, Amsterdam, Netherlands
[37] Nikhef National Institute for Subatomic Physics and VU University Amsterdam, Amsterdam, Netherlands
[38] AGH — University of Krakow, Faculty of Physics and Applied Computer Science, Kraków, Poland
[39] Henryk Niewodniczanski Institute of Nuclear Physics Polish Academy of Sciences, Kraków, Poland
[40] National Center for Nuclear Research (NCBJ), Warsaw, Poland
[41] Horia Hulubei National Institute of Physics and Nuclear Engineering, Bucharest-Magurele, Romania
[42] Affiliated with an institute covered by a cooperation agreement with CERN
[43] DS4DS, La Salle, Universitat Ramon Llull, Barcelona, Spain
[44] ICCUB, Universitat de Barcelona, Barcelona, Spain
[45] Instituto Galego de Física de Altas Enerxías (IGFAE), Universidade de Santiago de Compostela, Santiago de Compostela, Spain
[46] Instituto de Fisica Corpuscular, Centro Mixto Universidad de Valencia — CSIC, Valencia, Spain
[47] European Organization for Nuclear Research (CERN), Geneva, Switzerland
[48] Institute of Physics, Ecole Polytechnique Fédérale de Lausanne (EPFL), Lausanne, Switzerland
[49] Physik-Institut, Universität Zürich, Zürich, Switzerland
[50] NSC Kharkiv Institute of Physics and Technology (NSC KIPT), Kharkiv, Ukraine
[51] Institute for Nuclear Research of the National Academy of Sciences (KINR), Kyiv, Ukraine
[52] University of Birmingham, Birmingham, United Kingdom
[53] H.H. Wills Physics Laboratory, University of Bristol, Bristol, United Kingdom
[54] Cavendish Laboratory, University of Cambridge, Cambridge, United Kingdom
[55] Department of Physics, University of Warwick, Coventry, United Kingdom
[56] STFC Rutherford Appleton Laboratory, Didcot, United Kingdom
[57] School of Physics and Astronomy, University of Edinburgh, Edinburgh, United Kingdom
[58] School of Physics and Astronomy, University of Glasgow, Glasgow, United Kingdom
[59] Oliver Lodge Laboratory, University of Liverpool, Liverpool, United Kingdom
[60] Imperial College London, London, United Kingdom
[61] Department of Physics and Astronomy, University of Manchester, Manchester, United Kingdom
[62] Department of Physics, University of Oxford, Oxford, United Kingdom
[63] Massachusetts Institute of Technology, Cambridge, MA, United States
[64] University of Cincinnati, Cincinnati, OH, United States
[65] University of Maryland, College Park, MD, United States

JHEP04(2024)111

[66] Los Alamos National Laboratory (LANL), Los Alamos, NM, United States
[67] Syracuse University, Syracuse, NY, United States
[68] Pontifícia Universidade Católica do Rio de Janeiro (PUC-Rio), Rio de Janeiro, Brazil, associated to [3]
[69] School of Physics and Electronics, Hunan University, Changsha City, China, associated to [8]
[70] Guangdong Provincial Key Laboratory of Nuclear Science, Guangdong-Hong Kong Joint Laboratory of Quantum Matter, Institute of Quantum Matter, South China Normal University, Guangzhou, China, associated to [4]
[71] Lanzhou University, Lanzhou, China, associated to [5]
[72] School of Physics and Technology, Wuhan University, Wuhan, China, associated to [4]
[73] Departamento de Fisica, Universidad Nacional de Colombia, Bogota, Colombia, associated to [16]
[74] Universität Bonn — Helmholtz-Institut für Strahlen und Kernphysik, Bonn, Germany, associated to [20]
[75] Eotvos Lorand University, Budapest, Hungary, associated to [47]
[76] Van Swinderen Institute, University of Groningen, Groningen, Netherlands, associated to [36]
[77] Universiteit Maastricht, Maastricht, Netherlands, associated to [36]
[78] Tadeusz Kosciuszko Cracow University of Technology, Cracow, Poland, associated to [39]
[79] Department of Physics and Astronomy, Uppsala University, Uppsala, Sweden, associated to [58]
[80] University of Michigan, Ann Arbor, MI, United States, associated to [67]
[81] Departement de Physique Nucleaire (SPhN), Gif-Sur-Yvette, France

[a] Universidade de Brasília, Brasília, Brazil
[b] Centro Federal de Educacão Tecnológica Celso Suckow da Fonseca, Rio De Janeiro, Brazil
[c] Hangzhou Institute for Advanced Study, UCAS, Hangzhou, China
[d] LIP6, Sorbonne Universite, Paris, France
[e] Excellence Cluster ORIGINS, Munich, Germany
[f] Universidad Nacional Autónoma de Honduras, Tegucigalpa, Honduras
[g] Università di Bari, Bari, Italy
[h] Università di Bologna, Bologna, Italy
[i] Università di Cagliari, Cagliari, Italy
[j] Università di Ferrara, Ferrara, Italy
[k] Università di Firenze, Firenze, Italy
[l] Università di Genova, Genova, Italy
[m] Università degli Studi di Milano, Milano, Italy
[n] Università di Milano Bicocca, Milano, Italy
[o] Università di Padova, Padova, Italy
[p] Università di Perugia, Perugia, Italy
[q] Scuola Normale Superiore, Pisa, Italy
[r] Università di Pisa, Pisa, Italy
[s] Università della Basilicata, Potenza, Italy
[t] Università di Roma Tor Vergata, Roma, Italy
[u] Università di Siena, Siena, Italy
[v] Università di Urbino, Urbino, Italy
[w] Universidad de Alcalá, Alcalá de Henares, Spain
[x] Universidade da Coruña, Coruña, Spain
[y] Department of Physics/Division of Particle Physics, Lund, Sweden
[†] Deceased

JHEP04(2024)111